Modeling the horizon-absorbed gravitational flux for equatorial-circular orbits in Kerr spacetime

Andrea Taracchini, Alessandra Buonanno, Scott A. Hughes, and Gaurav Khanna

Phys. Rev. D **88**, 044001 — Published 1 August 2013

DOI: 10.1103/PhysRevD.88.044001

Modeling the horizon-absorbed gravitational flux for equatorial-circular orbits in Kerr spacetime

Andrea Taracchini,[1] Alessandra Buonanno,[1] Scott A. Hughes,[2,3,4] and Gaurav Khanna[5]

[1] *Maryland Center for Fundamental Physics & Joint Space-Science Institute, Department of Physics, University of Maryland, College Park, MD 20742, USA*
[2] *Department of Physics and MIT Kavli Institute, 77 Massachusetts Avenue, Cambridge, MA 02139*
[3] *Canadian Institute for Theoretical Astrophysics, University of Toronto, 60 St. George St., Toronto, ON M5S 3H8, Canada*
[4] *Perimeter Institute for Theoretical Physics, Waterloo, ON N2L 2Y5, Canada*
[5] *Department of Physics, University of Massachusetts Dartmouth, North Dartmouth, MA 02747*

We propose an improved analytical model for the horizon-absorbed gravitational-wave energy flux of a small body in circular orbit in the equatorial plane of a Kerr black hole. Post-Newtonian (PN) theory provides an analytical description of the multipolar components of the absorption flux through Taylor expansions in the orbital frequency. Building on previous work, we construct a mode-by-mode factorization of the absorbed flux whose Taylor expansion agrees with current PN results. This factorized form significantly improves the agreement with numerical results obtained with a frequency-domain Teukolsky code, which evolves through a sequence of circular orbits up to the photon orbit. We perform the comparison between model and numerical data for dimensionless Kerr spins $-0.99 \leq q \leq 0.99$ and for frequencies up to the light ring of the Kerr black hole. Our proposed model enforces the presence of a zero in the flux at an orbital frequency equal to the frequency of the horizon, as predicted by perturbation theory. It also reproduces the expected divergence of the flux close to the light ring. Neither of these features are captured by the Taylor-expanded PN flux. Our proposed absorption flux can also help improve models for the inspiral, merger, ringdown of small mass-ratio binary systems.

PACS numbers: 04.25.D-, 04.25.dg, 04.25.Nx, 04.30.-w

I. INTRODUCTION

Extreme-mass-ratio inspirals (EMRIs) are among the most interesting candidate sources for future space-based gravitational wave (GW) detectors. In these systems a particle/small body, like a star or a black hole (BH), orbits a supermassive BH and spirals in due to energy losses in GWs. Computational modeling of EMRIs is uniquely challenging due to the long duration and the high level of accuracy required in the waveforms for the purposes of detection [1]. This implies that the orbital dynamics needs to be computed over long time intervals with sufficient accuracy. To lowest order in the mass ratio, EMRIs can be described using black hole perturbation theory to compute how the "self force" produced by the small body interacts with its own spacetime deformation (see, e.g., Refs. [2, 3] for recent reviews). If the system evolves slowly enough, the impact of *dissipative* self forces can be described using the Teukolsky equation [4] to compute the slowly-changing evolution of the integrals of Kerr geodesic orbits (i.e., an orbit's energy, angular momentum, and Carter constant). The inspiral is then well described by a slowly evolving sequence of geodesic orbits. In Refs. [5–10], this approach has been pursued through purely numerical schemes.

Purely analytical approaches and modeling are also viable. Since the motion of the particle eventually becomes significantly relativistic, a post-Newtonian (PN) treatment [11–13] of this problem (taking the limit of small mass ratio) is bound to fail towards the end of the inspiral. In fact, PN theory used for long-time integration of EMRIs leads to significant discrepancies in the number of orbital cycles. These accumulate rather uniformly during the inspiral, even before reaching the innermost stable circular orbit (ISCO) [14]. More suitable approaches are BH perturbation theory and the self-force formalism [3, 4], which include all relativistic effects but expand in the small mass-ratio parameter.

In this work we focus on a specific aspect of the problem, namely the GW energy flux absorbed by the BH horizon. The particle orbiting the central Kerr BH radiates GWs which partly leave the binary towards null infinity (and constitute the so-called flux at infinity), and partly fall into the event horizon (and constitute the so-called absorption flux). Interest in the absorption flux was shown as early as the 70's, when Ref. [15] investigated its possible impact on the dynamics of bodies in the vicinity of the supermassive BH at the center of our galaxy.

For some orbits and black-hole spins, the absorption of GWs by the event horizon can be described as a Penrose-like process [16], i.e., as the extraction of rotational energy of the Kerr BH by means of negative-energy GWs. The "absorbed" flux in these cases is actually negative. Reference [17] formally suggested this Penrose-like interpretation for scalar (instead of gravitational) perturbations of a Kerr BH using the Teukolsky equation. The authors also looked for orbits which would have a perfect balance between the energy losses in scalar waves to infinity and the aforementioned energy extraction. Such orbits would have a constant radius, and were named

"floating orbits"[1]. Subsequently, Ref. [19] extended the calculation of the ingoing energy flux to gravitational perturbations of a Kerr BH [see in particular Eq. (4.44) therein], and computed it numerically for different values of the spin of the central object [see Fig. 2 in Ref. [19]]. Reference [20] later definitively ruled out the existence of floating orbits in the case of gravitational perturbations. More recent work [21] suggests that floating orbits can only exist around central bodies with an extremely unusual multipolar structure. In the context of alternative theories of gravity, it was shown [22] that floating is possible when massive scalar fields coupled to matter are present.

Further insight into the horizon-absorbed flux in a BH binary system can be gained from a parallel with the phenomenon of tides. For a recent review, see Ref. [23]. In the early 70's, Refs. [24, 25] computed how a stationary particle tidally perturbs a slowly rotating Kerr BH, finding that the BH dissipates energy by spinning down. The same phenomenon happens in a Newtonian binary system, such as when a moon perturbs a slowly rotating planet (treated as a fluid body with viscosity). This phenomenon is known as "tidal heating." Somewhat remarkably, there is a close analogy between the spindown of a black hole and the spindown of a fluid body due to the tidal interaction: The tidal interaction raises a bulge on the black hole's event horizon, and one can regard that bulge as exerting a torque on the orbit. This torque spins up or spins down the hole, depending on the relative frequency of the orbit and the hole's rotation. Using the membrane paradigm [26], one can even associate an effective viscosity to the black hole. The hole's viscosity relates the rate at which the horizon's generators are sheared to the rate at which the hole's area (or entropy) is increased. The black hole's viscosity plays an important role in determining the geometry of the hole's bulge, much as the viscosity of a fluid body in part determines the geometry of its tidal bulge.

A renewed interest in the BH-absorption flux was rekindled in the 90's, when, using BH perturbation theory, Ref. [27] computed in full analytical form the leading-order absorption flux for a particle in circular orbit around a Schwarzschild BH. These initial results indicated that the horizon flux is suppressed relative to the flux to infinity by a factor of v^8, where v is the orbital speed. This result was then generalized to the spinning case in Refs. [28, 29], where the ingoing flux was computed up to 6.5PN order beyond the leading order luminosity at infinity. Spin dramatically changes the leading impact of the horizon flux: The suppression factor becomes $(v^3 - q)v^5$ (where $q \equiv a/M$ is the Kerr parameter per unit mass). Numerical studies of strong field radiation reaction showed that neglect of the horizon flux would introduce large errors into Kerr inspiral models — many thousands of radians for inspiral into rapidly rotating black holes [6].

The extension to comparable-mass BH binaries was first attempted in Ref. [30], which computed the changes in mass and angular momentum of the holes up to 4PN order beyond the leading order luminosity at infinity. Reference [31] constructed a general approach to this problem, deriving formulae for the flow of energy and angular momentum into a BH as functions of the generic tidal fields perturbing it. This formalism was applied in Ref. [32] to the specific tidal environment of a comparable-mass binary in the slow-motion approximation, allowing the computation of the spinning absorption fluxes to higher PN order than Ref. [30]. Recently Ref. [33] pushed the calculation of Ref. [32] to an even higher PN order. Recent numerical work [34] found horizon absorption to be crucial in the ultrarelativistic grazing collision of comparable-mass BHs, in that it puts a limit on the maximum radiation that can be produced in such events.

In recent years, significant effort has been put into improving the analytical modeling of the GW fluxes, both ingoing and at infinity, with respect to the exact, numerical solution of the Teukolsky equation. In particular, Refs. [35, 36] proposed a factorization of the Taylor-expanded PN formulae for the flux at infinity in the Schwarzschild case, improving the agreement with the numerical data. Reference [37] extended this approach to the spinning case. Later on Ref. [38] applied the same idea of factorizing the PN Taylor-expanded PN predictions to the absorption flux in the nonspinning limit, extending the model also to comparable-mass binaries. Our work has the primary goal of studying the factorization of the BH-absorption flux for the Kerr case. The orbits we consider are circular and lie in the equatorial plane of the central, rotating BH. The PN-expanded formulae for the spinning absorption flux can be found in Refs. [28, 29].

An improved analytical modeling of the GW fluxes in the test-particle limit is crucial because of the practical need for fast generation of reliable time-domain waveforms for these systems. Several papers [39–44] have already incorporated analytical fluxes into effective-one-body (EOB) models for EMRIs. One solves the Hamilton equations for the Kerr Hamiltonian with dissipation effects introduced through a radiation-reaction force that is proportional to the GW flux. As far as the ingoing flux is concerned, Ref. [41] worked with spinning EMRIs, including the BH-absorption terms in Taylor-expanded PN form [28, 29]. The authors of Ref. [44] focussed on the nonspinning case, and used the factorized nonspinning absorption flux of Ref. [38]. Our work can be regarded as a step beyond Ref. [41] toward building a high-quality EOB model for EMRIs with spinning black holes. Besides the specific problem of the long inspiral in EMRIs, the EOB model has proven effective in describing the whole process of inspiral, merger and ringdown — for example Ref. [45] has used the results of this work to

[1] Similar behavior was noted by Hod in the context of massive-scalar fields, so-called "stationary clouds" [18].

model merger waveforms from small mass-ratio binary systems for any BH spin.

This paper is organized as follows. In Sec. II we discuss the numerical computation of energy fluxes at infinity and into the BH horizon using the frequency-domain Teukolsky equation. We investigate the behavior of these fluxes close to the photon orbit, discussing their main features. In Sec. III we review the factorization of the analytical GW fluxes computed in PN theory and apply it to the spinning BH-absorption flux. In Sec. IV we show comparisons of the factorized and Taylor-expanded PN fluxes to the numerical fluxes. In Sec. V we conclude and discuss future research. Appendix A discusses in more depth aspects of the near-light-ring fluxes, in particular how these fluxes diverge at the photon orbit, and how this divergence can be analytically factored from the fluxes. Appendix B contains the explicit formulae for a particular choice of the factorization model of the BH-absorption flux. Lastly, in Appendices C and D we provide fits to the Teukolsky-equation fluxes that can be employed for accurate evolution of EMRIs or inspiral, merger and ringdown waveforms for small mass-ratio binary systems.

Throughout this paper, we use geometrized units with $G = c = 1$. We use μ to label the mass of the small body; M and $q \equiv a/M$ are the mass and dimensionless spin of the Kerr black hole, respectively. The spin parameter q ranges from -1 to $+1$, with positive values describing prograde orbits, and negative values retrograde ones. With this convention, the orbital angular momentum L_z and orbital frequency Ω are always positive. When we discuss radiation and fluxes, we will often decompose it into modes. Through most of the paper, we decompose the radiation using spheroidal harmonics $S_{\ell m\omega}(\theta,\phi)$, discussed in more detail in Sec. II. In Sec. III, we will find it useful to use an alternative decomposition into spherical harmonics, $Y_{lm}(\theta,\phi)$. We will strictly use the harmonic indices (ℓ, m) for spheroidal harmonics, and (l, m) for spherical harmonics.

II. NUMERICAL COMPUTATION OF THE GRAVITATIONAL-WAVE FLUXES

In this section we first outline how we numerically compute GW fluxes (both ingoing and at infinity) by solving the frequency-domain Teukolsky equation. Much of this has been described in detail in other papers, in particular, Refs. [5, 7], so our discussion just highlights aspects which are crucial to this paper. Then, we discuss the main characteristics of those fluxes, their strength as function of the spin and their behavior close to the photon orbit.

A. Synopsis of numerical method

The Teukolsky "master" equation is a partial differential equation in Boyer-Lindquist coordinates r, θ, and t (the axial dependence is trivially separated as $e^{im\phi}$). It describes the evolution of perturbing fields of spin weight s to a Kerr black hole [4]. The equation for $s = -2$ describes the curvature perturbation ψ_4, a projection of the Weyl curvature tensor which represents outgoing radiation. With some manipulation, solutions for $s = -2$ give radiation at the hole's event horizon as well [19].

The master equation for $s = -2$ separates by introducing the multipolar decomposition

$$\psi_4 = \frac{1}{(r - iMq\cos\theta)^4}\int_{-\infty}^{\infty} d\omega \times \sum_{\ell m} R_{\ell m\omega}(r) S^{-}_{\ell m\omega}(\theta,\phi) e^{-i\omega t} \,. \quad (1)$$

Here and elsewhere in this paper, any sum over ℓ and m is taken to run over $2 \le \ell < \infty$, and $-\ell \le m \le \ell$, unless explicitly indicated otherwise. The function $S^{-}_{\ell m\omega}(\theta,\phi)$ is a spheroidal harmonic of spin-weight -2; the minus superscript is a reminder of this spin weight. It reduces to the spin-weighted spherical harmonic when $qM\omega = 0$: $S^{-}_{\ell m\omega}(\theta,\phi) = Y^{-}_{\ell m}(\theta,\phi)$ in this limit. The radial dependence $R_{\ell m\omega}(r)$ is governed by the equation

$$\Delta^2 \frac{d}{dr}\left(\frac{1}{\Delta}\frac{dR_{\ell m\omega}}{dr}\right) - V(r) R_{\ell m\omega} = -\mathcal{T}_{\ell m\omega}(r) \,. \quad (2)$$

The quantity $\Delta = r^2 - 2Mr + M^2q^2$, and the potential $V(r)$ can be found in Refs. [5, 7]. Note that in Eqs. (1), (2), (3), and (4), the variable r labels the coordinate of an arbitrary field point. This is true only in these specific equations; elsewhere in this paper, r gives the radius of a circular orbit.

Equation (2) is often called the frequency-domain Teukolsky equation, or just the Teukolsky equation. The source $\mathcal{T}_{\ell m\omega}(r)$ is built from certain projections of the stress-energy tensor for a small body orbiting the black hole:

$$T_{\alpha\beta} = \frac{\mu u_\alpha u_\beta}{\Sigma \sin\theta (dt/d\tau)} \delta[r - r_{\rm o}(t)]\delta[\theta - \theta_{\rm o}(t)]\delta[\phi - \phi_{\rm o}(t)] \,. \quad (3)$$

The subscript "o" means "orbit," and labels the coordinates of an orbiting body's worldline. We focus on circular equatorial orbits, so $\theta_{\rm o}(t) = \pi/2$, and $r_{\rm o}(t) =$ constant. Notice the factor $(dt/d\tau)^{-1}$ that appears here. As the light ring (LR) is approached, $dt/d\tau \to 0$, and this factor introduces a pole into the energy fluxes. We discuss the importance of this pole in more detail below, and describe how it can be analytically factored from the fluxes in Appendix A.

We consider orbits from $r_{\rm o}$ near the light ring out to very large radius ($r_{\rm o} \simeq 10^4 M$). Previous work has typically only considered orbits down to the ISCO. However, our code can solve Eq. (2) for any bound orbit, including unstable ones[2]. No modifications are needed to broaden

[2] In Ref. [41], we stated that our code did not work inside the

our study to these extremely strong-field cases, though there are some important considerations regarding convergence, which we discuss below.

We solve Eq. (2) by building a Green's function from solutions to the homogeneous equation (i.e., with $\mathcal{T}_{\ell m\omega} = 0$) and then integrating over the source; see Refs. [5, 7] for details. The resulting solutions have the form

$$R_{\ell m\omega}(r) = \begin{cases} Z^{\rm H}_{\ell m\omega} R^{\infty}_{\ell m\omega}(r) & r \to \infty, \\ Z^{\infty}_{\ell m\omega} R^{\rm H}_{\ell m\omega}(r) & r \to r_+, \end{cases} \tag{4}$$

where

$$Z^{\rm H}_{\ell m\omega} = C^{\rm H} \int_{r_+}^{r_{\rm orb}} dr' \frac{R^{\rm H}_{\ell m\omega}(r')\mathcal{T}_{\ell m\omega}(r')}{\Delta(r')^2} , \tag{5}$$

$$Z^{\infty}_{\ell m\omega} = C^{\infty} \int_{r_{\rm orb}}^{\infty} dr' \frac{R^{\infty}_{\ell m\omega}(r')\mathcal{T}_{\ell m\omega}(r')}{\Delta(r')^2} , \tag{6}$$

and where $R^{\star}_{\ell m\omega}(r)$ are the homogeneous solutions from which we build the Green's function ($\star$ means ∞ or H, as appropriate). The symbol $C^{\star}$ is shorthand for a collection of constants whose detailed form is not needed here (see Sec. III of Ref. [7] for further discussion).

The code we use to compute these quantities is described in Refs. [5, 7], updated to use the methods introduced by Fujita and Tagoshi [46, 47] (see also Ref. [11]). This method expands the homogeneous Teukolsky solutions as a series of hypergeometric functions, with the coefficients of these series determined by a three term recurrence relation, Eq. (123) of Ref. [11]. Successfully finding these coefficients requires that we first compute a number ν which determines the root of a continued fraction equation, Eq. (2.16) of Ref. [46]. Provided we can find ν, we generally find very accurate[3] solutions for $R^{\star}_{lm\omega}$. However, there are some cases, very close to the light ring and for $\ell \gtrsim 60$, in which our code fails to find a solution for ν. In these cases, the root of the continued fraction lies so close to a pole of this equation that our root finder cannot distinguish root from pole. (Figures 4 and 5 of Ref. [46] show examples of the pole and root structure of this equation for less problematic cases.) We discuss where this limitation impacts our analysis below.

For periodic orbits, the coefficients $Z^{\star}_{\ell m\omega}$ have a discrete spectrum:

$$Z^{\star}_{\ell m\omega} = Z^{\star}_{\ell m}\delta(\omega - \omega_m) , \tag{7}$$

where $\omega_m = m\Omega$, with Ω the orbital frequency of the small body. The amplitudes $Z^{\star}_{\ell m}$ then completely determine the fluxes of energy and angular momentum:

$$\dot{E}^{\infty} = \sum_{\ell m} \frac{|Z^{\rm H}_{\ell m}|^2}{4\pi\omega_m^2} \equiv \sum_{\ell m} F^{\infty}_{\ell m,{\rm Teuk}} = F^{\infty}_{\rm Teuk} , \tag{8}$$

$$\dot{E}^{\rm H} = \sum_{\ell m} \frac{\alpha_{\ell m}|Z^{\infty}_{\ell m}|^2}{4\pi\omega_m^2} \equiv \sum_{\ell m} F^{\rm H}_{\ell m,{\rm Teuk}} = F^{\rm H}_{\rm Teuk} . \tag{9}$$

For circular and equatorial orbits, fluxes of angular momentum are simply related to energy fluxes: $\dot{E}^{\star} = \Omega\dot{L}^{\star}$.

The factor $\alpha_{\ell m}$ which appears in fluxes on the horizon arises from converting the curvature scalar ψ_4 to ψ_0 in order to determine, via the area theorem, the rate at which the black hole's mass and spin change due to tidal coupling with the orbiting body (see Ref. [19] for discussion). The fluxes carried by radiation are then determined by imposing global conservation of energy and angular momentum[4]. This factor is given by

$$\alpha_{\ell m} = \frac{256(2Mr_+)^5 p_m(p_m^2+4\epsilon^2)(p_m^2+16\epsilon^2)\omega_m^3}{|c_{\ell m}|^2} , \tag{10}$$

where $r_+/M = 1+\sqrt{1-q^2}$ and $M\Omega_{\rm H} = q/(2r_+)$ are the radial position and frequency of the event horizon, $p_m = \omega_m - m\Omega_{\rm H}$, $\epsilon = \sqrt{1-q^2}/(4r_+)$, and

$$\begin{aligned} |c_{\ell m}|^2 &= \left[(\lambda+2)^2 + 4qM\omega_m - 4q^2M^2\omega_m^2\right] \\ &\times (\lambda^2 + 36mqM\omega_m - 36q^2M^2\omega_m^2) \\ &+ (2\lambda+3)(96q^2M^2\omega_m^2 - 48mqM\omega_m) \\ &+ 144M^2\omega_m^2(1-q^2) . \end{aligned} \tag{11}$$

In this quantity,

$$\lambda = \mathcal{E}_{\ell m} - 2qMm\omega_m + q^2M^2\omega_m^2 - 2 . \tag{12}$$

(Note that the subscript was incorrectly left off of ω_m when λ was defined in Ref. [41].) The number $\mathcal{E}_{\ell m}$ is the eigenvalue of the spheroidal harmonic; in the Schwarzschild limit, it reduces to $\ell(\ell+1)$. Notice that $\alpha_{\ell m} \propto p_m \propto (\Omega - \Omega_H)$. This means that the horizon flux is negative when $\Omega < \Omega_H$, consistent with the leading order result, Eq. (21).

All the data computed with these methods will be referred to as "numerical data" in the rest of the paper.

ISCO because there are no stable orbits there. It is true that we cannot relate the fluxes to quantities like the rate of change of orbital radius, inside the ISCO, but the code can compute fluxes from unstable orbits perfectly well in this regime.

[3] We estimate our solutions to have a fractional error $\sim 10^{-14}$ in these cases. R. Fujita has provided numerical data computed with an independent Teukolsky solver. We find 15 or more digits of agreement in our computed amplitudes in all cases.

[4] Our ability to use these conservation laws follows from the fact that the Kerr spacetime admits timelike and axial Killing vectors.

B. Discretization of orbits and convergence of the flux sums

We compute these fluxes on a pair of grids evenly spaced in the velocity variable

$$v \equiv (M\Omega)^{1/3} = \left[(r/M)^{3/2} + q\right]^{-1/3} . \qquad (13)$$

(In this section and beyond, there is no longer an ambiguity between labels for field point or orbital radius. In the remainder of the paper, r will label the radius of a circular orbit.) Our "outer" grid consists of 10^4 points spaced from $v = 0.01$ ($r \simeq 10^4 M$) to the ISCO radius [48],

$$\begin{aligned} \frac{r_{\rm ISCO}}{M} &= 3 + Z_2 \mp \sqrt{(3-Z_1)(3+Z_1+2Z_2)} , \\ Z_1 &= 1 + (1-q^2)^{1/3}\left[(1+q)^{1/3} + (1-q)^{1/3}\right] , \\ Z_2 &= (3q^2 + Z_1^2)^{1/2} . \end{aligned} \qquad (14)$$

[The upper sign in Eq. (14) is for prograde orbits, $q > 0$, and the lower for retrograde, $q < 0$.] Our "inner" grid consists of 100 points spaced from the ISCO to just outside the light ring: $r_{\rm min} = r_{\rm LR} + 0.01M$, where [48]

$$\frac{r_{\rm LR}}{M} = 2\left[1 + \cos\left(\frac{2}{3}\arccos(-q)\right)\right] . \qquad (15)$$

In some cases, we put $r_{\rm min} = r_{\rm LR} + 0.009M$. This is to avoid the problem mentioned in the text following Eq. (6): For very strong-field (large Ω) orbits, when $\ell \gtrsim 60$, we sometimes find a value of $m\Omega$ for which we cannot find the number ν, and hence cannot solve the Teukolsky equation. The cause of this difficulty, as mentioned above, is that we compute ν by finding a root of a particular continued fraction equation, Eq. (2.16) of Ref. [46]. This equation also has several poles. When $m\Omega$ and ℓ are large, the roots and poles can be so close to one another than they cannot be distinguished at double precision, and this method fails for that multipole. This (rather annoying) behavior will be discussed in more detail in a forthcoming paper [49]. For our purposes, it suffices to note that we find empirically that modifying the grid slightly to avoid those problematic frequencies fixes this problem.

For circular, equatorial orbits, the largest contributions to the sums for $F^\star$ tend to come at small ℓ (usually $\ell = 2$), and then fall off as explained in Eq. (18) as we go to higher values of ℓ. We consider a sum to have "converged" when we reach a value $\ell \equiv \ell_{\rm max}$ such that the fractional change in the sum due to all terms with $\ell = \ell_{\rm max}$ is smaller than 10^{-14} for three consecutive values of ℓ. This criterion was also used in Ref. [41]. For all orbits up to and including the ISCO, we were able to achieve this convergence for every spin that we examined. However, the $\ell_{\rm max}$ needed varies considerably with spin, mostly because the location of the ISCO varies strongly with spin: The deeper into the strong field we must go, the more multipoles are needed for convergence. For Schwarzschild, convergence required going to $\ell_{\rm max} = 30$ at the ISCO. For prograde $q = 0.99$, the same level of convergence took us to $\ell_{\rm max} = 66$ at the ISCO.

We were unable to achieve this convergence criterion for all orbits inside the ISCO. As we approach the light ring, the falloff of contributions to the flux sums becomes shallow, and the number of multipoles needed to converge becomes extremely large. At our innermost gridpoint $r_{\rm min}$, for $\ell \sim 70$ we find

$$\frac{F^\star_\ell}{F^\star_{\ell-1}} \simeq 1 - \epsilon , \qquad (16)$$

where $F^\star_\ell \equiv \sum_m F^\star_{\ell m}$, $\epsilon \approx$ a few $\times\, 0.01$. This is consistent with past analytical work on geodesic synchrotron radiation [50–53] which showed that a similar flux quantity (defined by summing over all allowed values of ℓ for a fixed m) is proportional to $(m_{\rm c}/m)\exp(-2m/m_{\rm c})$, where

$$m_{\rm c} \equiv \frac{2\sqrt{3}}{\pi}\frac{r_{\rm LR}/M + 3}{\sqrt{r_{\rm LR}/M}}\left(\frac{E}{\mu}\right)^2 , \qquad (17)$$

and E is the binding energy for circular orbits given in Eq. (29), which diverges at the light ring as $(r - r_{\rm LR})^{-1/2}$. The sums are dominated by the $\ell = |m|$ contributions, so either limiting form — $(m_{\rm c}/m)\exp(-2m/m_{\rm c})$ or $(\ell_{\rm c}/\ell)\exp(-2\ell/\ell_{\rm c})$ — is accurate. In our case, we find

$$F^\infty_\ell \propto \frac{(E/\mu)^2}{\ell}\exp\left[-2\ell\left(\frac{r}{r_{\rm LR}} - 1\right)\right], \qquad (18)$$

where E is the energy of the circular orbit at radius r, given by Eq. (29) below. It was shown that the same result holds also for the absorption flux for orbits close to the photon orbit. When $r = r_{\rm min}$ the exponential factor is ≈ 1 up to $\ell \sim \mathcal{O}((r_{\rm min} - r_{\rm LR})^{-1}) \gtrsim 100$, which is consistent with the behavior described by Eq. (16). These flux sums would converge eventually if we computed enough multipolar contributions. However, at very large values of ℓ and m, the methods we use to solve for the homogeneous Teukolsky solutions $R^\star_{\ell m\omega}(r)$ fail to find a solution. For all prograde orbits, we terminate the flux sums at $\ell = 70$ if the convergence criterion has not been met at this point. Large q retrograde orbits are more of a challenge; we have difficulty computing these modes (for the reasons discussed in Sec. II A above) for somewhat smaller values of ℓ for large, negative q. We terminate our sums when we cannot reliably compute $R^\star_{\ell m\omega}(r)$. The value of ℓ we reach is shown in Table I, and varies from 70 for $q = -0.5$ to 43 for $q = -0.99$.

To understand how much error we incur by terminating these sums, we examine how the flux behaves at the innermost grid point at $\ell_{\rm max}$ and $\ell_{\rm max} - 1$. The fractional error due to the multipoles which have been neglected in our sum is

$$\varepsilon^\star_{\rm negl} \equiv \frac{1}{F^\star}\sum_{\ell=\ell_{\rm max}+1}^{\infty} F^\star_\ell . \qquad (19)$$

q	$\ell_{\rm max}$	$F^{\infty}_{\ell=\ell_{\rm max}}/F^{\infty}$	$F^{\rm H}_{\ell=\ell_{\rm max}}/F^{\rm H}$	$\varepsilon^{\infty}_{\rm negl}$	$\varepsilon^{\rm H}_{\rm negl}$
0.99	70	7.06×10^{-5}	6.78×10^{-9}	0.0398%	3.82×10^{-6}%
0.9	70	6.93×10^{-4}	2.28×10^{-4}	1.10%	0.36%
0.7	70	1.38×10^{-3}	1.17×10^{-3}	3.54%	3.00%
0.5	70	1.49×10^{-3}	1.44×10^{-3}	4.80%	4.64%
0.0	70	1.82×10^{-3}	2.04×10^{-3}	8.07%	9.05%
−0.5	70	2.03×10^{-3}	2.36×10^{-3}	10.9%	12.7%
−0.7	66	2.31×10^{-3}	2.71×10^{-3}	13.1%	15.4%
−0.9	56	3.10×10^{-3}	3.68×10^{-3}	18.1%	21.5%
−0.99	43	4.75×10^{-3}	5.66×10^{-3}	23.5%	28.1%

TABLE I: Diagnostics of convergence at our innermost gridpoint, $r_{\rm min}=r_{\rm LR}+0.01M$, where the convergence is poorest. The second column lists the $\ell_{\rm max}$ where we end the sums for the total fluxes $F^{\star}$. The third column shows the flux to infinity in all $\ell=\ell_{\rm max}$ modes, normalized to the total flux (all modes up to and including $\ell=\ell_{\rm max}$). The third column is the same data for the horizon flux. The fourth and fifth columns give the error measure $\varepsilon^{\star}_{\rm negl}$, defined by Eq. (20). Convergence rapidly improves as we move away from this radius, with errors falling to 10^{-14} at radii a few $\times\,0.1M$ from the light ring.

If we assume that $F^{\star}_{\ell}$ falls off as suggested by Eq. (18) for $\ell\gtrsim\ell_{\rm max}$, this error can be estimated to be

$$\begin{aligned}\varepsilon^{\star}_{\rm negl} &= \frac{F^{\star}_{\ell_{\rm max}}}{F^{\star}}\left[\frac{F^{\star}_{\ell_{\rm max}+1}}{F^{\star}_{\ell_{\rm max}}}+\frac{F^{\star}_{\ell_{\rm max}+2}}{F^{\star}_{\ell_{\rm max}}}+\cdots\right]\\ &\leq \frac{F^{\star}_{\ell_{\rm max}}}{F^{\star}}\sum_{\ell=\ell_{\rm max}+1}^{\infty}\left(\frac{F^{\star}_{\ell}}{F^{\star}_{\ell-1}}\right)^{\ell-\ell_{\rm max}}\\ &= \frac{F^{\star}_{\ell_{\rm max}}}{F^{\star}}\sum_{\ell=\ell_{\rm max}+1}^{\infty}\left(\frac{\ell-1}{\ell}e^{-2/\ell_{\rm c}}\right)^{\ell-\ell_{\rm max}}\,. \qquad (20)\end{aligned}$$

Equation (20) is quite simple to compute, and is accurate enough for our purposes.

Table I summarizes how the fluxes behave at our innermost data point for all the spins we have examined. We see that $\varepsilon_{\rm negl}$ varies from less than a percent to about 20–30% at the innermost grid point in our study. The largest errors are for the high spin retrograde cases, where we are forced to terminate the sum relatively early.

These errors improve very rapidly as we move away from the light ring. For the case of $q=-0.99$ (the case with the largest errors due to neglected modes in our study), the contribution at $r\simeq r_{\rm LR}+0.05M$ has $F^{\infty}_{\ell_{\rm max}}/F^{\infty}\simeq1.16\times10^{-3}$, and $F^{\infty}_{\ell_{\rm max}}/F^{\infty}_{\ell_{\rm max}-1}\simeq0.930$; similar values describe the horizon flux at this location. Our rough estimate of the error falls to about 1.5%, an order of magnitude smaller than at our innermost grid point. We typically find that neglected terms in the sum contribute less than 10^{-14} to the total by the time we are a few $\times\,0.1M$ out from the light ring.

As was mentioned in the text following Eq. (3), the factor of $(dt/d\tau)^{-1}$ in the point-particle stress energy tensor introduces a pole in the fluxes, leading to strong divergence as a power of $1/(v-v_{\rm LR})$ as we approach the light ring. We have confirmed this behavior on a mode-by-mode basis, and have studied it using a modified version of our code in which this behavior is analytically factored from the fluxes (see Appendix A). Our numerical data up to $r_{\rm min}$ are consistent with a divergence of the total fluxes of the form $\sim(E/\mu)^2$.

It is worth emphasizing that if we use the WKB approximation [50–53] and normalize the fluxes (at infinity or through the BH horizon) to the specific energy and compute them exactly at the LR, we have $\left[F^{\star}_{\ell}/(E/\mu)^2\right]_{r_{\rm LR}}\sim1/\ell$. Thus, in the WKB approximation the total normalized fluxes diverge logarithmically when computed at the LR. A similar divergence was also found by Ref. [54] in the case of plunging orbits in Schwarzschild spacetime with an impact parameter fine-tuned next to the LR (see in particular Fig. 12 therein); for ultrarelativistic infalls the authors also saw a scaling of the radiated energy with E^2.

C. Features of numerical fluxes

We now analyze the numerical fluxes and describe their main features to gain insight for the analytical modeling.

In Boyer-Lindquist coordinates, at leading order in the PN expansion or Newtonian order, the ingoing GW flux reads [see, e.g., Eq. (11) in Ref. [30]]

$$F^{\rm H,\,N}=\frac{32}{5}\frac{\mu^2M^6}{r^6}\Omega\left(\Omega-\Omega_{\rm H}\right)\,, \qquad (21)$$

where r is the radial separation and Ω is the orbital frequency of the particle. This can be compared to the leading-order luminosity at infinity in GWs [13]

$$F^{\infty,\,\rm N}=\frac{32}{5}\mu^2r^4\Omega^6\,. \qquad (22)$$

For quasi-circular inspiral, Eqs. (21) and (22) tell us that $F^{\rm H,\,N}/F^{\infty,\,\rm N}\sim(M\Omega)^{5/3}$ for $q\neq0$, so the horizon flux is 2.5PN orders beyond the flux to infinity. In the nonspinning limit, $F^{\rm H,\,N}/F^{\infty,\,\rm N}\sim(M\Omega)^{8/3}$ — 4PN order in this case. Note that to obtain these ratios we used Eq. (13).

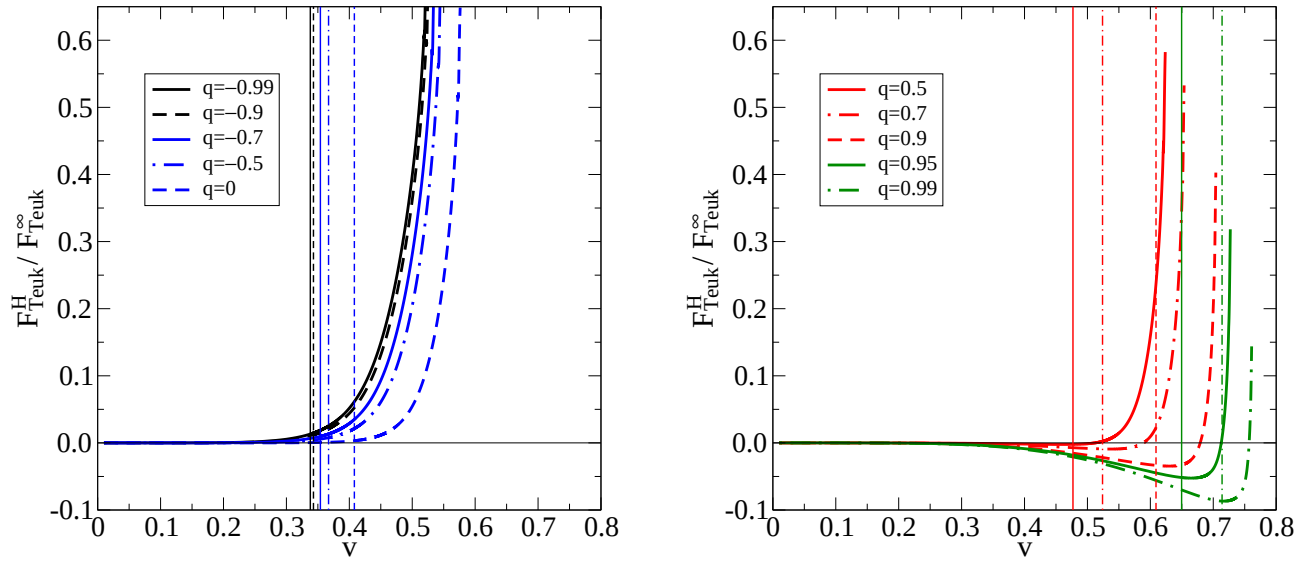

FIG. 1: We show the ratio between the energy flux absorbed by the horizon $F^{\rm H}$ and the energy flux radiated to infinity F^{∞} for different possible values of the spin q, as a function of $v \equiv (M\Omega)^{1/3}$. The data come from the numerical solution of the Teukolsky equation in the adiabatic approximation. All plots extend up to $r = r_{\rm LR} + 0.01M$. Vertical lines mark the positions of the respective ISCOs.

Thus, at leading order the absorption flux is suppressed with respect to the flux at infinity by $\mathcal{O}((M\Omega)^{5/3})$ for $q \neq 0$ or by $\mathcal{O}((M\Omega)^{8/3})$ for $q = 0$. In order to have a more accurate assessment of the relative importance of $F^{\rm H}$ and F^{∞}, in Fig. 1 we plot the ratio between the numerical fluxes at infinity and into the horizon $F^{\rm H}/F^{\infty}$ versus orbital velocity[5] for different values of the spin q. All curves in this figure extend up to a point just outside their respective equatorial LRs; the decreasing trend of $F^{\rm H}/F^{\infty}$ as a function of q is primarily due to how the factor $\Omega(\Omega-\Omega_{\rm H})$ behaves at the LR. We indicate the position of the respective ISCOs with vertical lines. For convenience, we list in Table II the position of the ISCOs and LRs expressed in terms of v for the spin cases considered in this paper.

In Ref. [41] [see Fig. 2 therein] the authors considered the total numerical flux $F^{\infty}_{\rm Teuk}+F^{\rm H}_{\rm Teuk}$ computed with the Teukolsky equation up to the ISCO for different spins, and compared it to a flux model where F^{∞} is the factorized flux of Ref. [37] and $F^{\rm H}$ is the Taylor-expanded PN flux of Refs. [28, 29]. They found that the inclusion of the analytical ingoing flux is crucial for improving agreement with the Teukolsky solution during the very long inspiral, implying that $F^{\rm H}$ is a significant fraction of F^{∞}. Our numerical data extend the analysis of Ref. [41] to more extreme spins (up to 0.99) and higher frequencies (up to the LRs). Figure 1 shows that $F^{\rm H}$ is typically a few percent of F^{∞} at the ISCO for $q \leq 0.7$, increasing to 8.7% when $q = 0.99$.

Another important feature that Fig. 1 shows is that $F^{\rm H}$ changes sign for $q > 0$ ($F^{\infty} > 0$ in all cases). Orbits for which $F^{\rm H}/F^{\infty} < 0$ are called "superradiant." They can be interpreted as due to a Penrose-like mechanism [16] in which the rotational energy of the BH is extracted. The change of sign of $F^{\rm H}$ for $q > 0$ can be understood by noticing that the sign of each mode $F^{\rm H}_{\ell m}$ is fixed by its specific structure in BH perturbation theory [see Eq. (10)]

$$F^{\rm H}_{\ell m} = m^2 \Omega \left(\Omega - \Omega_{\rm H}\right) \tilde{F}^{\rm H}_{\ell m} \,, \tag{23}$$

where $\tilde{F}^{\rm H}_{\ell m} > 0$. If $q > 0$, $\Omega_{\rm H} > 0$ as well, so when $0 < \Omega < \Omega_{\rm H}$, we have $F^{\rm H}_{\ell m} < 0$. This means that the particle gains energy through the GW modes with that specific value of m. Zeros in $F^{\rm H}$ for $q > 0$ in Fig. 1 coincide with the horizon velocities: $v_{\rm H} \equiv (M\Omega_{\rm H})^{1/3}$. We notice that for $q > 0$, an inspiraling test particle will always go through the zero of $F^{\rm H}$. In fact, the test-particle's velocity reaches its maximum value, which is always larger than $v_{\rm H}$, during the plunge. Afterwards, the test-particle's velocity decreases and gets locked to that of the horizon [45].

As discussed in the Introduction and as can be seen in Fig. 1, we always have $|F^{\rm H}|/F^{\infty} < 1$, meaning that we find no so-called "floating orbits." Although superradiance of the down-horizon modes does not allow for floating orbits, these modes nonetheless have a strong impact on inspiral. Comparing an inspiral that includes both $F^{\rm H}$ and F^{∞} with one that is driven only by F^{∞}, one finds that these modes make inspiral last longer, radiating additional cycles before the final plunge [41]. A

[5] Our $v \equiv (M\Omega)^{1/3}$ should not be confused with $v = (M/r)^{1/2}$ used in Ref. [29]. These definitions only agree when $q = 0$.

q	-0.99	-0.9	-0.7	-0.5	0	0.5	0.7	0.9	0.95	0.99
$v_{\rm ISCO}$	0.338	0.343	0.354	0.367	0.408	0.477	0.524	0.609	0.650	0.714
$v_{\rm LR}$	0.523	0.527	0.536	0.546	0.577	0.625	0.655	0.706	0.729	0.763

TABLE II: We show the orbital velocities corresponding to the positions of ISCO and LR for different values of the spin.

more quantitative assessment of this delayed merger can be found for instance in the nonspinning limit in Ref. [44]. In that work, the authors considered EOB orbital evolutions which include the horizon flux model developed in Ref. [38]. For $\mu/M = 10^{-3}$, they found that neglecting the horizon flux induces a dephasing of 1.6 rads for the (2,2) mode waveform h_{22} at merger over an evolution of about 41 orbital cycles. They also studied what happens for larger mass ratios, since their flux model worked even in the comparable-mass limit. However, in this regime the effects are much smaller, with a (2,2) mode dephasing of only 5×10^{-3} rads at merger cumulated over 15 orbits. This result is consistent with the estimations of Ref. [30], which considered a comparable-mass spinning case under a leading-order PN evolution.

In the case of spinning binaries with extreme mass-ratio, Refs. [5, 55] found that in the nearly extremal case $q = 0.998$ the last few hundred days of inspiral at mass ratio 10^{-6} are augmented by $\sim 5\%$ at low inclinations, depending on whether the ingoing flux is included or not. Using the exact Teukolsky-equation fluxes of this paper in the EOB equations of motion, Ref. [45] (see Table I therein) computed how the number of orbital cycles within a fixed radial range before the LR is affected by the addition of ingoing flux. Several different values of the spin were considered. For prograde orbits, the ingoing flux can increase the number of cycles by as much as $\sim 7\%$ for $q = 0.99$, which corresponds to about 45 rads of GW dephasing in the (2,2) mode over 100 GW cycles. On the other hand, for retrograde orbits or nonspinning black holes, the horizon flux tends to make inspiral faster, decreasing the number of cycles before plunge thanks to the additional loss of energy absorbed by the horizon in these cases. The horizon flux changes the duration of inspiral by at most $\sim 1\%$ when $q = -0.99$, a somewhat less significant effect.

Since we are going to model the multipolar modes $F^{\rm H}_{\ell m}$ rather than the total ingoing GW flux $F^{\rm H}$, it is useful to understand their relative importance. In Figs. 2 and 3 we show the ratio between the first few subdominant modes and the dominant (2,2) mode $F^{\rm H}_{22}$ as a function of the orbital velocity for the two extremal spin cases $q = \pm 0.99$. For $q = -0.99$ we note that at the ISCO the most important subdominant modes are the (3,3) and the (2,1), and they are both only a few percents of the dominant (2,2) mode. For $q = 0.99$, at the ISCO the subdominant modes which are at least 1% of the (2,2) mode are many more: (3,3), (4,4), (2,1), (5,5), (3,2) and (6,6). This is a general result: as the spin of the Kerr BH grows to large positive values, more and more multipolar

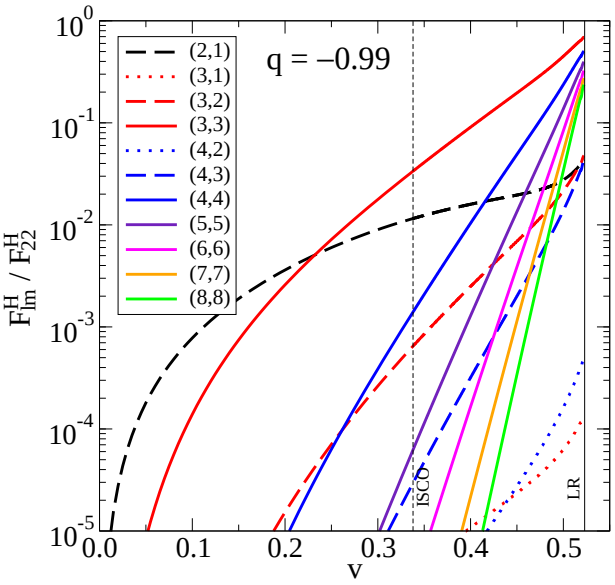

FIG. 2: We compare the Teukolsky-equation ingoing multipolar fluxes, normalized by the dominant mode $F^{\rm H}_{22}$, for spin $q = -0.99$. Vertical lines mark the position of the ISCO and the LR. The graphs extend up to $r = r_{\rm LR} + 0.01M$.

modes become important relative to the dominant (2,2) mode, even before the plunging phase, which starts after the crossing of the ISCO. Close to the LR all modes with $\ell = |m|$ become comparable to the (2,2) mode for both spins. This is similar to what happens for the multipolar decomposition of F^{∞} (see, e.g., Ref. [56]). Reference [43] already pointed out a similar behavior while discussing the spherical modes at infinity h_{lm}, which directly relate to the -2 spin-weighted spherical harmonic decomposition of F^{∞} [see Eq. (26) below].

A compact representation of the ratio $F^{\rm H}_{\ell m}/F^{\rm H}_{22}$ across the entire range of physical spins is given in Fig. 4. Choosing to evaluate the ratio at the same orbital frequency for different values of q would not be meaningful, since the position of the horizon changes with q, so we choose instead as common physical point the ISCO for all the spins. We see that at the ISCO the only modes which are consistently at least 1% of $F^{\rm H}_{22}$ are the (2,1) and (3,3) modes; only when $q \gtrsim 0.95$ the (4,4), (5,5), (6,6) and (3,2) modes are above 1% of the (2,2). Modes with $\ell = |m|$ appear to be evenly spaced on the logarithmic scale used for all spins. In other words, $F^{\rm H}_{\ell\ell}/F^{\rm H}_{22} \propto 10^{c(q)\ell}$,

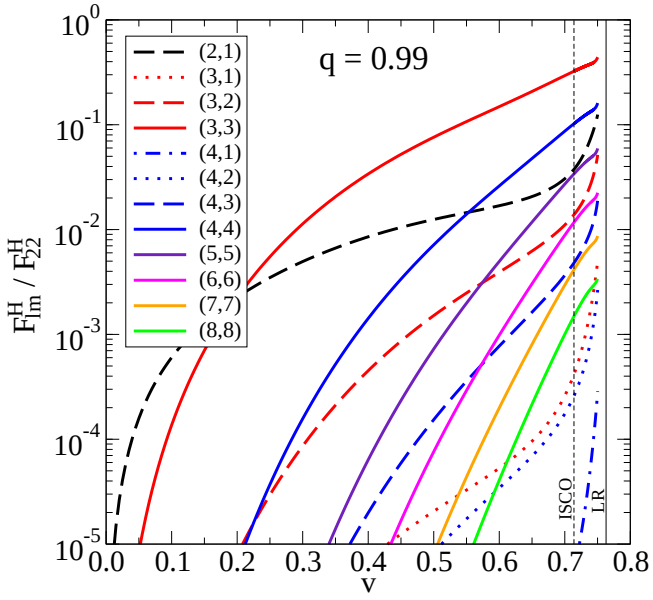

FIG. 3: We compare the Teukolsky-equation ingoing multipolar fluxes, normalized by the dominant mode $F^{\rm H}_{22}$, for spin $q = 0.99$. Vertical lines mark the position of the ISCO and the LR. The graphs extend up to $v \approx (M\Omega_{\rm H})^{1/3}$.

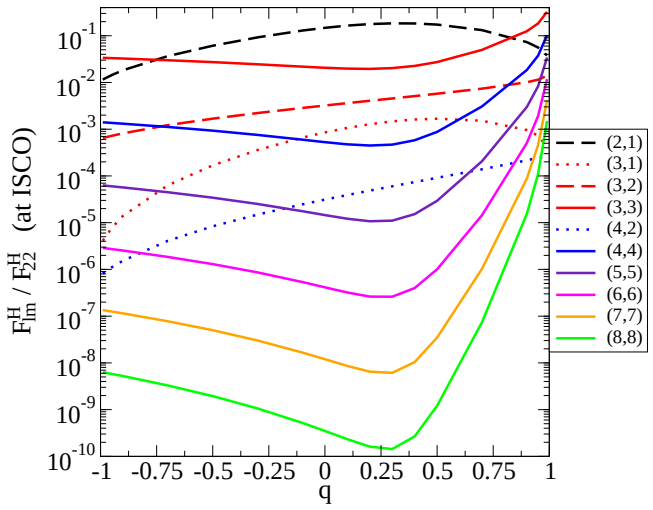

FIG. 4: We compare the Teukolsky-equation ingoing multipolar fluxes, normalized by the dominant mode $F^{\rm H}_{22}$, evaluated at the respective ISCOs.

where $c(q)$ is a spin-dependent constant[6]. We therefore do not see crossings among these modes as q varies between -1 and 1. On the other hand, we do see crossings between the largest subdominant modes, (2,1) and (3,3): when $-0.75 \lesssim q \lesssim 0.8$ we have $F^{\rm H}_{21} \geq F^{\rm H}_{33}$, otherwise (for almost extremal spins) $F^{\rm H}_{21} \leq F^{\rm H}_{33}$. The nature of these crossings seems to depend mostly on $|q|$, as it is also indirectly confirmed in Figs. 2 and 3, where the crossing of (2,1) and (3,3) (now considered in plots versus v at fixed q) occurs at a similar velocity $v \approx 0.2$ for both $q = -0.99$ and $q = 0.99$. A simple explanation of what we just discussed is the fact that, as q grows, the ISCO moves deeper into the strong field and the ISCO orbital velocity increases. In this circumstance, higher multipoles can become comparable in size to the (2,2) mode in spite of their higher PN order.

From Figs. 2-4 we also observe that, among modes with the same value of ℓ, the dominant ones are those with $\ell = |m|$, independently of the frequency. For the case of scalar perturbations of a Schwarzschild BH, Ref. [57] provided an analytical argument to account for this peculiar hierarchy. Within the WKB approximation (valid for $\ell \gg 1$) and for an orbit at $r \gg r_{\rm LR}$, it was shown that $F^{\infty}_{\ell m}/F^{\infty}_{\ell\ell} \propto \exp\left[-2C\left(\ell - |m|\right)\right]$, where C is a numerical constant which depends on r. As a consequence, nearly all of the power at infinity at a frequency $m\Omega$ is emitted in the $\ell = |m|$ modes. Similar arguments apply to the case of gravitational perturbations [51] and, more generally, to perturbations of a Kerr BH [52]. Explicitly, one finds that

$$F^{\infty}_{\ell m} \propto \exp\left[-2\int_{r^*_{\rm orb}}^{\bar{r}^*} \sqrt{V(r'^*) - m^2\Omega^2}\, {\rm d}r'^*\right]. \qquad (24)$$

Here, V is the radial potential seen by the perturbation, and r^* is the tortoise coordinate,

$$r^* = r + \frac{2Mr_+}{r_+ - r_-}\ln\left(\frac{r - r_+}{2M}\right) - \frac{2Mr_-}{r_+ - r_-}\ln\left(\frac{r - r_-}{2M}\right), \qquad (25)$$

where $r_\pm/M = 1 \pm \sqrt{1 - q^2}$. The integral's upper limit $\bar{r}^*$ is the larger of the two solutions to the equation $V(\bar{r}^*) = m^2\Omega^2$. Recall that Ω depends on r through Eq. (13). Note that $r^*_{\rm orb}$ is always smaller than $\bar{r}^*$. For a nonspinning BH and $\ell \gg 1$ the radial potential is the same regardless of the spin of the perturbing field [57], and reads $V(r) = \ell(\ell+1)(1 - 2M/r)/r^2$. Therefore the lower the value of m, the larger the value of $\bar{r}^*$, the larger the magnitude of the argument inside the exponential, and hence the larger the suppression. An analogous explanation applies to the absorption flux.

Finally, as we discussed in Sec. II B, the existence of a cutoff value $\ell_{\rm c}$ for sums over the flux modes reduces in practice the number of modes that contribute to the total flux. For orbits very close to the LR, $\ell_{\rm c}$ is a decreasing function of the spin. When $q \approx 1$ very few modes contribute, and the total flux is basically given by the (2,2) mode. This is consistent with Fig. 3, where in the strong-field region only the (3,3), (4,4) and (2,1) modes are at least 10% of the (2,2) mode. On the other hand, in Fig. 2 we can see that the (3,3), (4,4), (5,5), (6,6), (7,7) and (8,8) modes are all larger than 10% of the (2,2) mode at $r_{\rm min}$, and indeed the estimated $\ell_{\rm c}$ at that radial separation is ~ 200.

[6] This behavior is consistent with Eq. (16).

III. FACTORIZATION OF THE ENERGY FLUXES

The analytical representation of the ingoing flux in PN-expanded form provided in Ref. [29] turns out to be monotonic in the orbital frequency for all possible values of the spin, so that the sign-flip discussed above is not present. Moreover comparisons with the numerical fluxes (see Fig. 7) show that these PN formulae start performing poorly even before the ISCO, especially for large positive values of q. This is to be expected, since the ISCO moves to smaller radii (i.e. larger orbital frequencies) as q increases, that is outside the range of validity of the PN expansion; Ref. [58] attempted to determine the region of validity of the PN absorption flux more quantitatively. For instance, when $q = 0.9$, the Taylor-expanded PN model for $F^{\rm H}$ differs from the numerical data by more than 100% around an orbital velocity $v \approx 0.4$, while $v_{\rm ISCO} \approx 0.61$. An improved analytical model for $F^{\rm H}$ is therefore needed. In this section we will propose a factorization of the absorbed flux similar to what was done for the flux at infinity [35–38].

A. Factorization of the energy flux at infinity

For a particle spiraling in along an adiabatic sequence of circular orbits, the GW flux at infinity can be expressed as a sum over the waveform modes at infinity h_{lm}, as

$$F^{\infty} = \frac{M^2\Omega^2}{8\pi}\sum_{l=2}^{\infty}\sum_{m=1}^{l} m^2 \left|\frac{\mathcal{R}}{M}h_{lm}\right|^2 , \tag{26}$$

where $\mathcal{R}$ is the distance to the source. The mode decomposition here is done using the -2 spin-weighted spherical harmonics, rather than the spheroidal harmonics considered in the previous section; as discussed at the end of the introduction, the indices are labeled (l, m) rather than (ℓ, m) to flag this change of basis. In Ref. [35] a novel approach to improve the analytical modeling of the GW flux at infinity for a test particle in Schwarzschild was introduced. This approach was then generalized to spinning BHs in Ref. [37]. The idea is to start from the PN knowledge of h_{lm}, and recast the formulae, mode by mode, in a factorized form

$$h_{lm} \equiv h_{lm}^{(\rm N,\epsilon)} T_{lm} \hat{S}_{\rm eff}^{(\epsilon)} f_{lm} e^{i\delta_{lm}} , \tag{27}$$

where ϵ is either 0 if $l+m$ is even or 1 if $l+m$ is odd, $h_{lm}^{(\rm N,\epsilon)}$ is the leading order term, T_{lm} resums an infinite number of leading logarithms entering the tail effects, $\hat{S}_{\rm eff}^{(\epsilon)}$ is an effective source term which is divergent for circular motion at the LR, f_{lm} and δ_{lm} are polynomials in the variable v [see, e.g., Ref. [37] for more details]. The term f_{lm} is fixed by requiring that Eq. (31), when expanded in powers of v, agrees with the PN-expanded formulae. When computing the f_{lm}'s, one assumes quasi-circular orbits, and this is reflected by the choice of the source term,

$$\hat{S}_{\rm eff}^{(\epsilon)} = \begin{cases} \dfrac{E}{\mu}, & \text{if} \quad \epsilon = 0 \,, \\ \dfrac{L_z}{\mu M/v}, & \text{if} \quad \epsilon = 1 \,, \end{cases} \tag{28}$$

where E and L_z are the energy and angular momentum of a circular equatorial orbit in Kerr [48]

$$\frac{E}{\mu} = \frac{1 - 2M/r + q(M/r)^{3/2}}{\sqrt{1 - 3M/r + 2q(M/r)^{3/2}}} , \tag{29}$$

$$\frac{L_z}{\mu M} = \sqrt{\frac{r}{M}}\frac{1 - 2q(M/r)^{3/2} + q^2(M/r)^2}{\sqrt{1 - 3M/r + 2q(M/r)^{3/2}}} , \tag{30}$$

and $\mu M/v$ in the denominator of Eq. (28) is the Newtonian angular momentum for circular orbits. Note that this specific choice of the effective source term is not the only one possible. References [36, 37] also explored the possibility of using $\hat{S}_{\rm eff}^{(0)} = \hat{S}_{\rm eff}^{(1)} = E/\mu$, and labelled the resulting factorized odd-parity modes with the "H" superscript (meaning "Hamiltonian"), as opposed to the factorization done with the prescription in Eq. (28), whose odd-parity modes were labelled with the "L" superscript (meaning "angular momentum"). In the rest of the paper we are going to consider only the effective source of Eq. (28), and we will omit the "L" superscript.

Reference [36] found that the 1PN coefficient of the f_{lm} polynomials grows linearly with l, and therefore proposed a better-behaved factorization, namely

$$h_{lm} \equiv h_{lm}^{(\rm N,\epsilon)} T_{lm} \hat{S}_{\rm eff}^{(\epsilon)} (\rho_{lm})^l e^{i\delta_{lm}} , \tag{31}$$

where the f_{lm} factor is replaced by $(\rho_{lm})^l$. Both factorized representations of F^{∞} show an improved agreement with the numerical data with respect to PN approximants, as pointed out in Refs. [35, 36] for the nonspinning case and in Ref. [37] for the spinning case. Moreover, the ρ_{lm}–factorization turns out to perform better than the f_{lm}–factorization when compared with the Teukolsky-equation fluxes; this is discussed in more detail in Appendix C.

B. Factorization of the BH-absorption energy flux

Let us now consider the BH-absorption flux. For the special case of nonrotating BHs, Ref. [27] and Ref. [32] computed the lowest PN terms of $F^{\rm H}$, in the test-particle and comparable-mass limit, respectively. The spinning case was considered in Refs. [28, 29] in the test-particle limit and in Ref. [30] in the comparable-mass limit. In particular, Ref. [29] computed the PN expanded BH-absorption flux into a Kerr BH up to 6.5PN order beyond the leading order luminosity at infinity for circular orbits in the equatorial plane. The idea behind that calculation

is to solve the Teukolsky equation in two different limits, for separations $r \to \infty$ and for separations approaching the horizon, and then to match the two solutions in an intermediate region where both approximations are valid. These Taylor-expanded PN expressions are then decomposed into spheroidal[7] multipolar modes $F^{\rm H}_{\ell m}$, so that

$$F^{\rm H} = 2\sum_{\ell=2}^{\infty}\sum_{m=1}^{\ell} F^{\rm H}_{\ell m}\,, \tag{32}$$

where we used $F^{\rm H}_{\ell 0} = 0$ and $F^{\rm H}_{\ell m} \equiv F^{\rm H}_{\ell|m|}$. Note that this decomposition stems from the separation of variables of the Teukolsky equation in oblate spheroidal coordinates [19, 59].

Here, we count the PN orders with respect to the leading order luminosity at infinity of Eq. (22), which can be rewritten

$$F^{\infty,\,\rm N} = \frac{32}{5}\left(\frac{\mu}{M}\right)^2 v^{10}\,, \tag{33}$$

for circular orbits. Thus, as discussed above, for a nonspinning binary the leading order term in the BH-absorbed GW flux is 4PN [$\mathcal{O}(v^8)$ beyond the leading order luminosity at infinity], whereas for a Kerr BH it is 2.5PN [$\mathcal{O}(v^5)$ beyond the leading order luminosity at infinity].

Reference [38] considered the case of a nonspinning BH binary and applied a factorization to the multipolar ingoing GW flux, recasting it in the following form

$$F^{\rm H}_{\ell m} \equiv F^{\rm H,\,N}_{\ell m}(\hat{S}^{(\epsilon)}_{\rm eff})^2\left(\rho^{\rm H}_{\ell m}\right)^{2\ell}\,, \tag{34}$$

where $F^{\rm H,\,N}_{\ell m}$ is the nonspinning leading term, and $\rho^{\rm H}_{\ell m}$ is a polynomial in v determined by requiring that Eq. (34) agrees with the PN-expanded formulae from Refs. [27, 32] when expanded in powers of v. Here the "H" superscript refers to "horizon." Note that Ref. [38] defined the multipolar modes differently: their (ℓ, m) mode is the sum of our (ℓ, m) and $(\ell, -m)$ modes, so there is an overall factor 1/2. Reference [38] computed $\rho^{\rm H}_{22}$ up to 1PN order beyond $F^{\rm H,N}_{22}$ (i.e., 5PN order in our convention) in the Schwarzschild case and also in the comparable-mass case. However, in the Schwarzschild case, the total ingoing GW flux is actually known through 6PN order [29]

$$F^{\rm H}(q=0) = F^{\infty,\,\rm N} v^8\left[1 + 4v^2 + \frac{172}{7}v^4 + \mathcal{O}(v^5)\right]\,, \tag{35}$$

and specifically the individual mode $F^{\rm H}_{22}$ is known to the same PN order as $F^{\rm H}$, so that the factorization in Ref. [38] can be extended from 5PN to 6PN order (beyond the leading order luminosity at infinity).

Let us now consider the spinning case. As pointed out before, the Taylor-expanded PN form of the ingoing GW flux does not preserve the zero $(\Omega - \Omega_{\rm H})$, which is instead present in the exact expression of the $F^{\rm H}_{\ell m}$'s from BH perturbation theory. This means that, if we were to use a factorization like the one in Eq. (34) also for the Kerr case, our factorized flux would inherit this unwanted feature, since the factorization only tries to match the Taylor-expanded PN flux. Therefore, we propose the factorized form

$$F^{\rm H}_{\ell m} \equiv \left(1 - \frac{\Omega}{\Omega_{\rm H}}\right) F^{\rm H,\,N}_{\ell m}(\hat{S}^{(\epsilon)}_{\rm eff})^2(\tilde{f}^{\rm H}_{\ell m})^2\,, \tag{36}$$

which has the advantage of enforcing the presence of the zero at a frequency equal to $\Omega_{\rm H}$. The leading term is defined as

$$F^{\rm H,\,N}_{\ell m} \equiv \frac{32}{5}\left(\frac{\mu}{M}\right)^2 v^{7+4\ell+2\epsilon} n^{(\epsilon)}_{\ell m} c_{\ell m}(q)\,, \tag{37}$$

where

$$\begin{aligned} n^{(0)}_{\ell m} \;\equiv\; & -\frac{5}{32}\frac{(\ell+1)(\ell+2)}{\ell(\ell-1)}\frac{2\ell+1}{[(2\ell+1)!!]^2}\times \\ & \times\; \frac{(\ell-m)!}{[(\ell-m)!!]^2}\frac{(\ell+m)!}{[(\ell+m)!!]^2}\,, \end{aligned} \tag{38}$$

$$\begin{aligned} n^{(1)}_{\ell m} \;\equiv\; & -\frac{5}{8\ell^2}\frac{(\ell+1)(\ell+2)}{\ell(\ell-1)}\frac{2\ell+1}{[(2\ell+1)!!]^2}\times \\ & \times\; \frac{[(\ell-m)!!]^2}{(\ell-m)!}\frac{[(\ell+m)!!]^2}{(\ell+m)!}\,, \end{aligned} \tag{39}$$

and

$$\begin{aligned} c_{\ell m}(q) \;\equiv\; & \frac{1}{q}\prod_{k=0}^{\ell}\left[k^2 + \left(m^2 - k^2\right)q^2\right] = qm^2\left(1-q^2\right)^{\ell}\times \\ & \times\; \left(1 - \frac{imq}{\sqrt{1-q^2}}\right)_{\ell}\left(1 + \frac{imq}{\sqrt{1-q^2}}\right)_{\ell}\,, \end{aligned} \tag{40}$$

where $(z)_n \equiv z(z-1)\cdots(z-n+1)$ is the Pochhammer symbol. The factors $n^{(\epsilon)}_{\ell m}$ and $c_{\ell m}(q)$ allow the $\tilde{f}^{\rm H}_{\ell m}$'s to start with either 1 or 0. The definition of the factor $c_{\ell m}(q)$ is inspired by the derivation of the $\ell = 2$ modes in the slow-motion approximation in Ref. [31] [see Eq. (9.31) therein]. The definition of $n^{(\epsilon)}_{\ell m}$ is derived from Eqs. (5.17) and (5.18) in Ref. [27] (which considered the Schwarzschild case), but a few additional were factors included. These new factors are a prefactor of $1/(m\ell!)^2$ generated by our definition of $c_{\ell m}(q)$; a numerical factor of $-1/4$ due to the presence of $(1 - \Omega/\Omega_{\rm H})$ in Eq. (36); and a factor of 1/2 due to the definitions used in Ref. [27]. We also consider the factorization

$$F^{\rm H}_{\ell m} \equiv \left(1 - \frac{\Omega}{\Omega_{\rm H}}\right) F^{\rm H,\,N}_{\ell m}(\hat{S}^{(\epsilon)}_{\rm eff})^2\left(\tilde{\rho}^{\rm H}_{\ell m}\right)^{2\ell}\,, \tag{41}$$

where the factor $\tilde{f}^{\rm H}_{\ell m}$ in Eq. (36) is replaced by $\left(\tilde{\rho}^{\rm H}_{\ell m}\right)^{\ell}$, just as was done by Ref. [36] for F^{∞}. [Note that our $\tilde{\rho}_{\ell m}$'s are different from the $\rho_{\ell m}$'s in Ref. [38].]

[7] In this case, the modes are of spin-weight +2.

Appendix I of Ref. [29] lists the Taylor-expanded modes $F^{\rm H}_{\ell m}$ that are needed to compute the BH-absorption Taylor-expanded flux through 6.5PN order. Since the $F^{\rm H}_{\ell m}$'s in Ref. [29] are expressed in terms of the velocity parameter $(M/r)^{1/2}$ we use Eq. (13) to replace r with v. A straightforward but tedious calculation gives us the following expressions for the $\tilde{\rho}^{\rm H}_{\ell m}$ functions:

$$\begin{aligned}\tilde{\rho}^{\rm H}_{22} &= 1 + v^2 - \left\{2B_2 + \frac{q}{1+3q^2}\left[4 + \kappa\left(5+3q^2\right)\right]\right\}v^3 + \left(\frac{335}{84} - \frac{2}{21}q^2\right)v^4 \\ &- \left\{2B_2 + \frac{q}{1+3q^2}\left[\frac{47}{18} - \frac{25}{6}q^2 + \kappa\left(5+3q^2\right)\right]\right\}v^5 + \left\{\frac{293\,243}{14\,700} - \frac{2}{3}\pi^2 - \frac{6\,889}{1\,134}q^2 + \frac{3}{2}q^4 + 2B_2^2\right. \\ &+ 4C_2\left(1+\frac{2}{\kappa}\right) - \frac{428}{105}\left(A_2 + \gamma_E + \log 2 + \log\kappa + 2\log v\right) - \frac{1}{1+3q^2}\left[\frac{124}{9} - 8qB_2 - 2q\kappa B_2\left(5+3q^2\right)\right] \\ &\left.+ \frac{1}{\left(1+3q^2\right)^2}\left[\frac{56}{3} + 2\kappa\left(5 - 6q^2 + 3q^4 - 18q^6\right)\right]\right\}v^6 - \frac{1}{42}\left\{B_2\left(335 - 8q^2\right) + \frac{q}{1+3q^2}\left[\frac{1\,670}{3} - \frac{3\,131}{9}q^2 + \frac{73}{3}q^4\right.\right. \\ &\left.\left.+ \frac{\kappa}{2}\left(5+3q^2\right)\left(335 - 8q^2\right)\right]\right\}v^7 + \left\{\frac{6\,260\,459}{151\,200} - \frac{2}{3}\pi^2 - \frac{25\,234}{5\,292}q^2 + \frac{8\,439}{5\,292}q^4 - \frac{148}{7}\gamma_E - \frac{428}{105}A_2 + 2B_2^2\right. \\ &+ 4C_2\left(1+\frac{2}{\kappa}\right) - \frac{25}{9}qB_2 + \frac{1}{1+3q^2}\left[-\frac{322}{27} + 8qB_2 + 2\kappa qB_2\left(5+3q^2\right)\right] + \frac{1}{\left(1+3q^2\right)^2}\left[\frac{56}{3} + \kappa\left(10 - \frac{341}{18}q^2\right.\right. \\ &\left.\left.\left.- 19q^4 - \frac{97}{2}q^6\right)\right] - \frac{4\,012}{105}\log 2 - \frac{428}{105}\log\kappa - \frac{2\,648}{105}\log v\right\}v^8 + \mathcal{O}(v^9)\,, \end{aligned} \tag{42a}$$

$$\begin{aligned}\tilde{\rho}^{\rm H}_{21} &= 1 - \frac{q}{3}v + \left(\frac{7}{12} - \frac{q^2}{18}\right)v^2 - \left\{B_1 + \frac{1}{18}q\left(\frac{1}{3}q^2 - \frac{31}{2}\right) + \frac{q}{4-3q^2}\left[1 + \kappa\left(5-3q^2\right)\right]\right\}v^3 + \left\{\frac{521}{672} + \frac{1}{3}qB_1\right. \\ &\left.- q^2\left(\frac{1\,847}{1\,512} + \frac{5}{648}q^2\right) + \frac{1}{4-3q^2}\left[\frac{4}{9} + q^2\kappa\left(\frac{5}{3} - q^2\right)\right]\right\}v^4 + \left[-\frac{B_1}{36}\left(21 - 2q^2\right) - \frac{1}{4-3q^2}\left(-\frac{347}{72}q\right.\right. \\ &\left.\left.+ \frac{3\,053}{864}q^3 + \frac{703}{1\,944}q^5 - \frac{7}{648}q^7 + \frac{1}{36}\kappa q\left(21-2q^2\right)\left(5-3q^2\right)\right)\right]v^5 + \left\{\frac{267\,092\,969}{38\,102\,400} - \frac{32\,125}{12\,096}q^2 + \frac{81\,167}{54\,432}q^4\right. \\ &- \frac{7}{3\,888}q^6 - \frac{107}{105}\left(A_1 + \gamma_E + \log 2 + \log\kappa + 2\log v\right) + \frac{1}{2}B_1^2 + C_1\left(1+\frac{2}{\kappa}\right) - \frac{\pi^2}{6} - \frac{1}{4-3q^2}\left[\frac{298}{243}\right. \\ &\left.\left.+ qB_1\left(\frac{22}{9} - \frac{287}{108}q^2 + \frac{1}{18}q^4 - \kappa\left(5-3q^2\right)\right)\right] + \frac{1}{\left(4-3q^2\right)^2}\left[-\frac{4}{3} + \kappa\left(40 - \frac{1\,208}{9}q^2 + \frac{14\,539}{108}q^4\right.\right.\right. \\ &\left.\left.\left.- \frac{177}{4}q^6 + \frac{1}{6}q^8\right)\right]\right\}v^6 + \mathcal{O}(v^7)\,, \end{aligned} \tag{42b}$$

$$\begin{aligned}\tilde{\rho}^{\rm H}_{33} &= 1 + \frac{7}{6}v^2 - \left\{2B_3 + \frac{2q}{\left(1+8q^2\right)\left(4+5q^2\right)}\left[\frac{131}{9} + \frac{314}{9}q^2 - \frac{40}{9}q^4 + 3\kappa\left(5+13q^2\right)\right]\right\}v^3 \\ &+ \left(\frac{353}{120} - \frac{5}{18}q^2\right)v^4 + \mathcal{O}(v^5)\,, \end{aligned} \tag{43a}$$

$$\tilde{\rho}^{\rm H}_{32} = 1 - \frac{1}{4}qv + \left(\frac{5}{6} - \frac{1}{16}q^2\right)v^2 + \mathcal{O}(v^3)\,, \tag{43b}$$

$$\begin{aligned}\tilde{\rho}^{\rm H}_{31} &= 1 + \frac{29}{18}v^2 - \frac{2}{3}\left\{B_1 + \frac{q}{4-3q^2}\left[\kappa\left(5-3q^2\right) + \frac{1}{9-8q^2}\left(65 - \frac{866}{9}q^2 + \frac{104}{3}q^4\right)\right]\right\}v^3 \\ &+ \left(\frac{1\,903}{648} + \frac{1}{6}q^2\right)v^4 + \mathcal{O}(v^5)\,, \end{aligned} \tag{43c}$$

$$\tilde{\rho}^{\rm H}_{44} = 1 + \mathcal{O}(v)\,, \tag{44a}$$

$$\tilde{\rho}^{\rm H}_{43} = \mathcal{O}(v)\,, \tag{44b}$$

$$\tilde{\rho}^{\rm H}_{42} = 1 + \mathcal{O}(v)\,, \tag{44c}$$

$$\tilde{\rho}^{\rm H}_{41} = \mathcal{O}(v)\,. \tag{44d}$$

In these equations, $\gamma_E \approx 0.57721\ldots$ is the Euler-Mascheroni constant, $\kappa \equiv \sqrt{1-q^2}$, and

$$A_n \equiv \frac{1}{2}\left[\psi^{(0)}\left(3+\frac{inq}{\kappa}\right)+\psi^{(0)}\left(3-\frac{inq}{\kappa}\right)\right], \tag{45}$$

$$B_n \equiv \frac{1}{2i}\left[\psi^{(0)}\left(3+\frac{inq}{\kappa}\right)-\psi^{(0)}\left(3-\frac{inq}{\kappa}\right)\right], \tag{46}$$

$$C_n \equiv \frac{1}{2}\left[\psi^{(1)}\left(3+\frac{inq}{\kappa}\right)+\psi^{(1)}\left(3-\frac{inq}{\kappa}\right)\right]; \tag{47}$$

$\psi^{(n)}$ is the polygamma function.

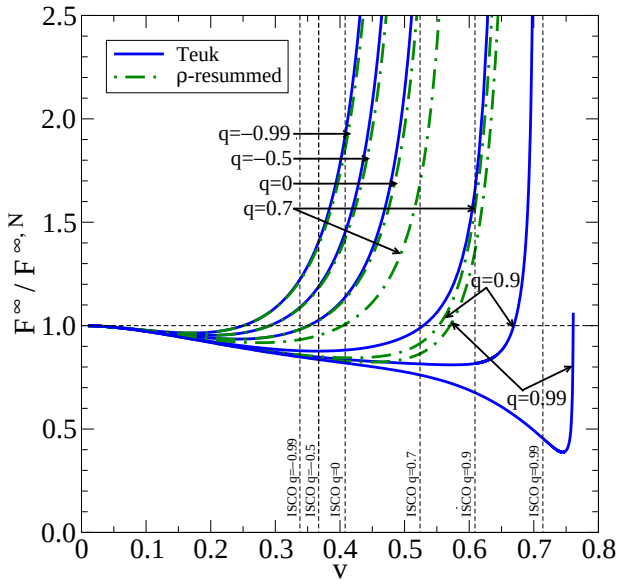

FIG. 5: We compare the Teukolsky-equation flux at infinity with the factorized flux of Ref. [37]. The computation is done up to the $r_{\rm LR}+0.01M$.

The explicit expressions of the $\tilde{f}^{\rm H}_{\ell m}$ functions can be found in Appendix B. Given the limited number of available modes in Taylor-expanded PN form, we are not able to convincingly argue that the $\tilde{\rho}^{\rm H}_{\ell m}$–factorization is preferable to the $\tilde{f}^{\rm H}_{\ell m}$–factorization on the basis of the growth with ℓ of the 1PN coefficient in the $\tilde{f}^{\rm H}_{\ell m}$'s, as done in Refs. [36, 37] for F^{∞}. We prefer the $\tilde{\rho}^{\rm H}_{\ell m}$–factorization over the $\tilde{f}^{\rm H}_{\ell m}$–factorization because we find that it compares better to the numerical data.

IV. COMPARISON WITH NUMERICAL RESULTS

In this section we compare the Teukolsky-equation fluxes (both at infinity and ingoing) to the analytical models discussed in Sec. III.

A. Comparison with the numerical flux at infinity

In Fig. 5 we show the Teukolsky-equation flux at infinity for several different spin values up to the LR and compare it to the factorized flux reviewed in Sec. III A and developed in Ref. [37]. We note that the factorized flux is fairly close to the numerical data until the LR for retrograde and nonspinning cases. For large spin prograde cases, the modeling error instead becomes large already at the ISCO[8]. Following the approach of Ref. [41], in Appendix C we have improved the factorized flux at infinity by fitting the $\rho_{\ell m}$'s to the Teukolsky-equation data. These fits can be useful for very accurate numerical evolution of PN or EOB equations of motions for EMRIs, and also for the merger modeling of small mass-ratio binary systems [45].

B. Comparison with the numerical flux through the black-hole horizon

In Fig. 6 we compare the BH-absorption Taylor-expanded PN flux from Ref. [29] and our factorized flux to the numerical flux produced with the frequency-domain Teukolsky equation, normalized to the leading order luminosity at infinity. In Fig. 7 we plot the fractional difference between numerical and factorized fluxes. The factorized model is quite effective in reproducing the numerical data, not only because we have factorized the zero $(1-\Omega/\Omega_H)$ in Eq. (36), but also because we have factorized the pole at the LR through the source term $\hat{S}^{(\epsilon)}_{\rm eff}$ in Eq. (36). As we see in Fig. 6, the factorized flux is quite close to the numerical flux up to $q \leq 0.5$, but starts performing not very well soon after the ISCO when $q \geq 0.7$, systematically underestimating $|F^{\rm H}|$ in the range $v_{\rm ISCO} < v < v_{\rm H}$ for large positive spins. As we see in Fig. 7, for spins $-1 \leq q \leq 0.5$ the agreement of the factorized model to the numerical data is better than 1% up to the ISCO, with a remarkable improvement over the Taylor-expanded PN model. For instance, for $q = 0.5$, the ISCO is located at $v_{\rm ISCO} \approx 0.48$. Up to the ISCO the agreement is below 1%, while in the last part of the frequency range (up to the LR) we see that the performance becomes worse. For larger spins the factorized model starts to visibly depart from the numerical data even before the ISCO, but the error is still within 50% at the ISCO for $q = 0.9$. By contrast, the Taylor-

[8] Besides the $\rho_{\ell m}$–factorization discussed in Sec. III A, Ref. [37] also proposed an improved resummation of the $\rho_{\ell m}$ polynomials, which consists in factoring out their 0.5PN, 1PN and 1.5PN order terms, with a significant improvement in the modeling error.

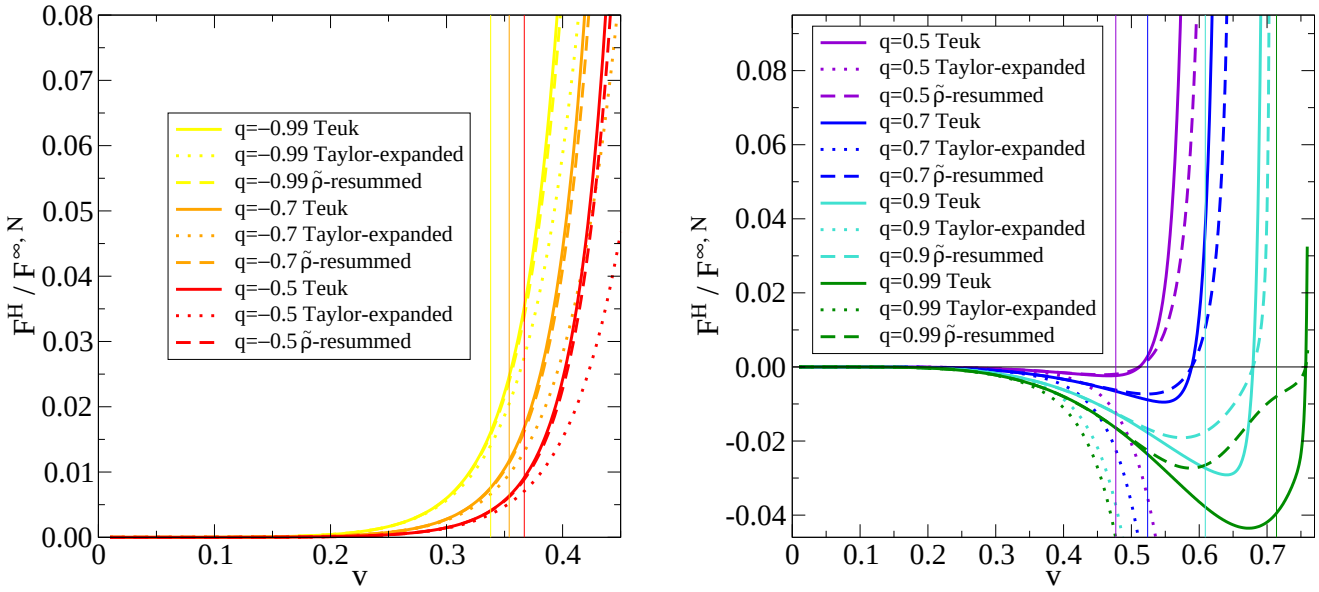

FIG. 6: We compare the Teukolsky-equation BH-absorption flux (solid lines) to the Taylor-expanded PN model of Ref. [29] (dotted lines) and the factorized flux proposed in this work (dashed lines), as functions of v. All curves extend up to $r = r_{\rm LR} + 0.01M$. Vertical lines mark the positions of the respective ISCOs. The fluxes are normalized to the leading order flux at infinity $F^{\infty,\rm N}$. In the left panel we show cases with $q < 0$, while in the right panel we show cases with $q > 0$.

expanded PN model is completely off. For positive spins we see that the relative error of the factorized model goes to zero at $v = (M\Omega_{\rm H})^{1/3} \equiv v_{\rm H}$, which is where our model by construction agrees with the Teukolsky-equation data thanks to the factor $(1 - \Omega/\Omega_{\rm H})$. On the other hand, the Taylor-expanded PN model has the wrong sign at high frequencies when $q > 0$.

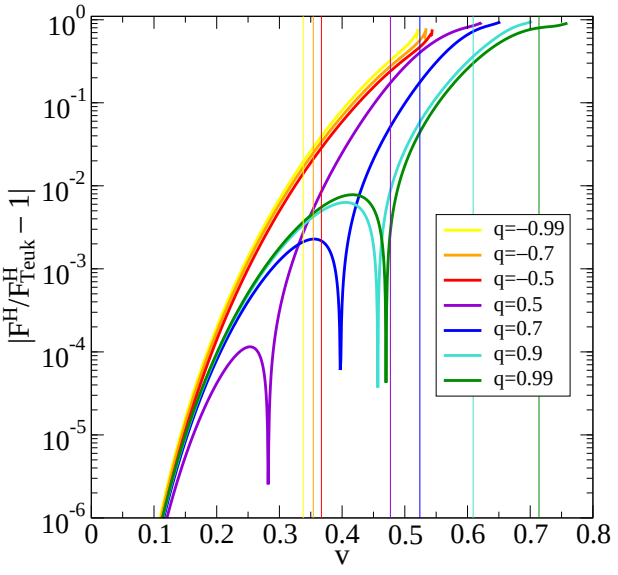

FIG. 7: We show the fractional difference between the total factorized and Teukolsky-equation fluxes. All curves extend up to the respective LRs. Vertical lines mark the positions of the respective ISCOs.

The large modeling error of the factorized flux for $q \geq 0.7$ after the ISCO should not be a reason for significant concern. Physical inspirals will not include circular motion beyond the ISCO; the main purpose of modeling fluxes from these orbits is to properly include the influence of this pole near the light ring. The physical motion will in fact transition to a rapid plunge near the ISCO, generating negligible flux. In Ref. [45], we evolved EOB equations of motions incorporating the absorption flux into the radiation reaction force. We found that using the exact Teukolsky-equation flux or the factorized model flux of this paper makes very little difference in terms of the duration of the inspiral. For the large spin cases (i.e., those with the largest modeling error even before the ISCO) the length of the inspiral varies by at most $\sim 0.5\%$. In any case, if higher modeling accuracy on $F^{\rm H}$ is needed, one can of course resort to a similar approach to what Refs. [38, 41] did for F^{∞}, namely fitting the numerical data. We pursue this task in Appendix D.

Let us now focus on the multipolar modes of the BH-absorption flux, rather than the total flux. In Figs. 8 and 9 we compare the dominant (2,2) mode and leading subdominant (2,1) mode. We only show the results for the $\tilde{\rho}^{\rm H}$–factorization, but comment also about the performance of the Taylor flux below. For the $\ell = 2$ modes, the relative error of our factorized model is at least one order of magnitude smaller than the Taylor-expanded PN model across the entire frequency range up to the LR. We also find that for the (3,3) mode the improvement of the factorized model over the Taylor-expanded PN model is more modest, especially at higher frequencies. For positive spins the Taylor-expanded PN (3,3) mode

has actually a comparable performance to the factorized flux. This can be explained from the fact that the analytical knowledge for $\ell = 3, 4$ modes is pretty limited [see Eqs. (I2)-(I7) in Ref. [29]], so that the two models cannot differ drastically.

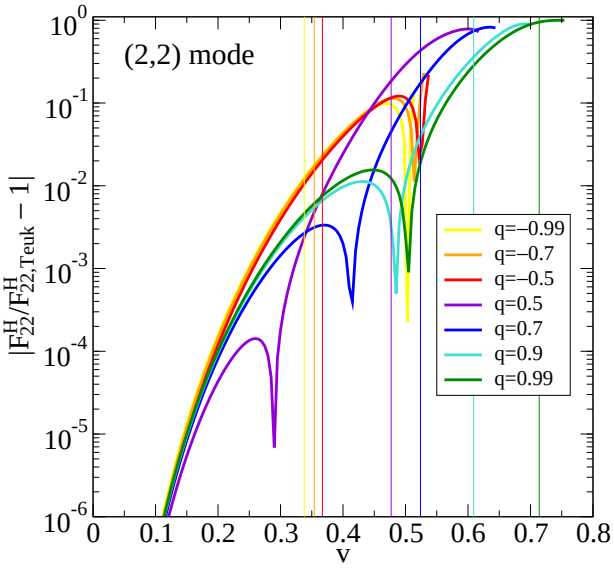

FIG. 8: We show the fractional error of our model with respect to the (2,2) mode of the Teukolsky-equation BH-absorption flux. All curves extend up to the respective LRs. Vertical lines mark the positions of the respective ISCOs.

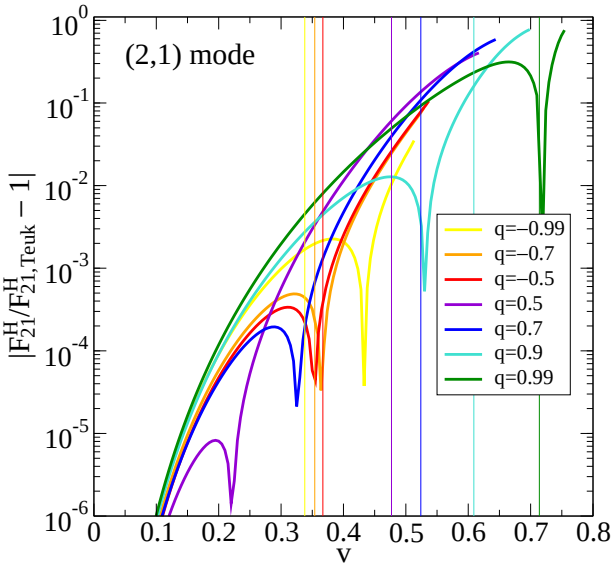

FIG. 9: We show the fractional error of our model with respect to the (2,1) mode of the Teukolsky-equation BH-absorption flux. All curves extend up to the respective LRs. Vertical lines mark the positions of the respective ISCOs.

As we have discussed, in the factorized approach, the main ingredient of modeling the absorption flux is the

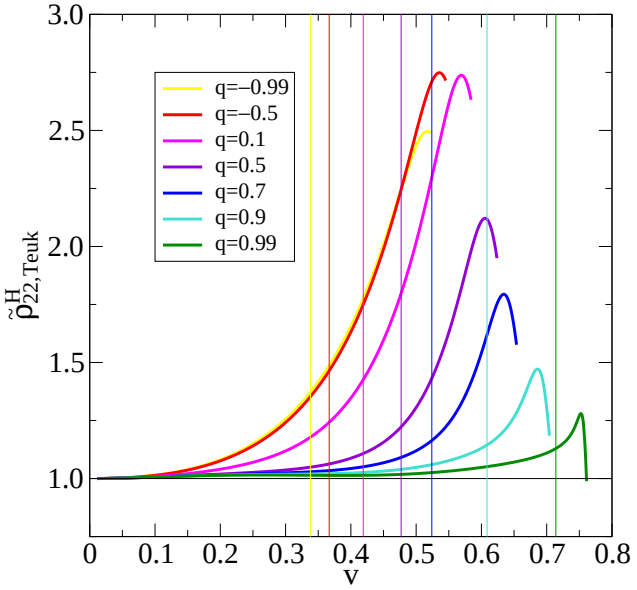

FIG. 10: We show the Teukolsky-equation $\tilde{\rho}^H_{22}$ as functions of v. All curves extend up to $r = r_{LR} + 0.01M$. As in the nonspinning case [38], also in the spinning case the Teukolsky-equation $\tilde{\rho}^H_{22}$ behaves non monotonically in the strong-field region close to the LS. This peculiar behavior cannot be easily captured by a polynomial model. This holds true also for other modes with $\ell = m$. On the other hand, the Teukolsky-equation $\tilde{\rho}^H_{\ell m}$'s for $\ell \neq |m|$ (e.g., the (2,1) mode) have monotonic dependence on v up to the LR. Vertical lines mark the positions of the respective ISCOs.

polynomial factor $\tilde{\rho}^H_{\ell m}$. Future progress in the PN knowledge of the analytical fluxes will directly translate into new, higher-order terms in the $\tilde{\rho}^H_{\ell m}$ polynomials. Therefore it is useful to explicitly compute the Teukolsky-equation $\tilde{\rho}^H_{\ell m,Teuk}$'s. We simply divide $F^H_{\ell m,Teuk}$ by the leading and source terms, and take the 2ℓ-th root. The result is shown in Fig. 10, only for the $\ell = 2$ modes. A peculiar feature (generically seen in all modes with $\ell = m$) is the peak in $\tilde{\rho}^H_{22,Teuk}$ in the strong-field regime, inside the ISCO and close to the LR. Such feature is completely missed by the polynomial model of Eq. (42a). Reference [38] noticed a similar shape in the nonspinning limit, using their ρ^H_{22} mode [defined through Eq. (34)], and proposed to fit it through a rational function. The $\tilde{\rho}^H_{21,Teuk}$'s do not display any relevant feature at high frequencies; this is the case also for all the other $\ell \neq |m|$ modes that we checked. In Appendix D we provide a more accurate analytical representation of the absorption flux by fitting the Teukolsky-equation flux F^H. These fits can be useful for very accurate numerical evolution of PN or EOB equations of motions for EMRIs, and also for the merger modeling of small mass-ratio binary systems [45].

C. Comparing black-hole absorption fluxes in the nonspinning case

Before ending this section we want to compare our nonspinning results to the numerical data and to the results of Ref. [38]. As discussed above, the BH-absorption Taylor-expanded PN flux is known through 6PN order beyond $F^{\infty,\,\mathrm{N}}$ [see Eq. (35)]. However, in Ref. [38], where the Schwarzschild case was considered, the authors used the Taylor-expanded PN flux only through 5PN order and, as a consequence, using Eq. (34) they computed the BH-absorption factorized flux only up to 5PN order. Using the full information contained in Refs. [28, 29] for the Taylor-expanded PN flux we obtain ρ^{H}_{22} through 6PN order, that is

$$\rho^{\mathrm{H}}_{22}(q=0) = 1 + v^2 + \frac{335}{84}v^4 + \mathcal{O}(v^6)\,. \qquad (48)$$

In Fig. 11 we show for $q=0$ the ρ^{H}_{22} extracted from the

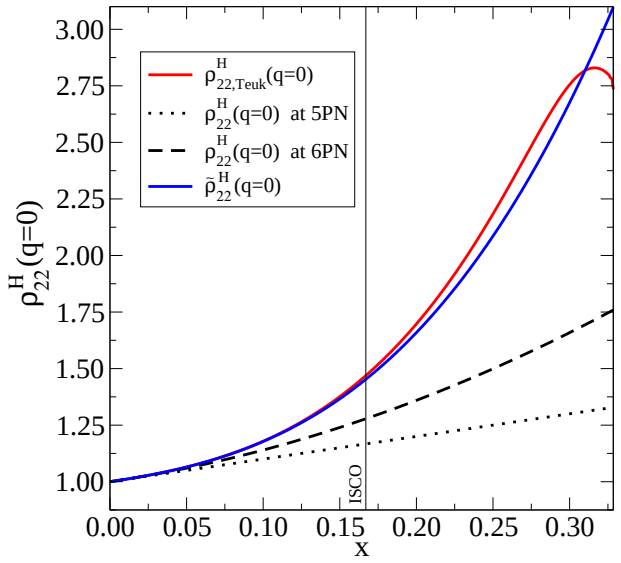

FIG. 11: We compare the nonspinning ρ^{H}_{22} computed from the Teukolsky-equation data of F^{H}_{22} with the nonspinning factorized flux derived in Ref. [38] up to 5PN order and in this paper up to 6PN order. We also include the nonspinning limit of the factorized flux $\tilde{\rho}^{\mathrm{H}}_{22}$ proposed in this paper. The curves are plotted against $x \equiv (M\Omega)^{2/3} = v^2$, and extend up to the LR in $x_{\mathrm{LR}} = 1/3$. A vertical line marks the ISCO in $x_{\mathrm{ISCO}} = 1/6$.

numerical data as

$$\rho^{\mathrm{H}}_{22,\,\mathrm{Teuk}}(q=0) \equiv \left[\frac{2F^{\mathrm{H}}_{22,\,\mathrm{Teuk}}(q=0)}{\frac{32}{5}\left(\frac{\mu}{M}\right)^2 v^{18}(\hat{S}^{(0)}_{\mathrm{eff}})^2}\right]^{1/4}, \qquad (49)$$

the ρ^{H}_{22} at 5PN and 6PN order from Eq. (48), and the nonspinning limit of the $\tilde{\rho}^{\mathrm{H}}_{22}$ proposed in this paper.

It is interesting to observe that our $\tilde{\rho}^{\mathrm{H}}_{22}$ is much closer to the numerical data than the ρ^{H}_{22}. We emphasize that in the nonspinning limit $\tilde{\rho}^{\mathrm{H}}_{22}$ contains higher-order PN terms produced by the factorization procedure, which singles out the zero $(1-\Omega/\Omega_H)$.

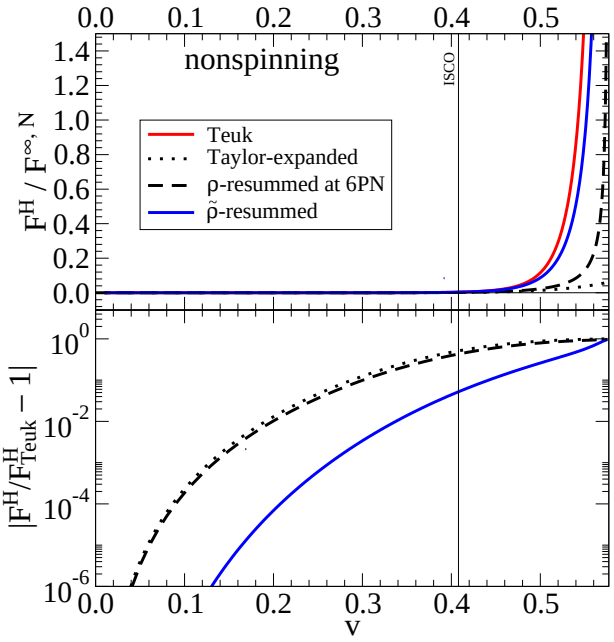

FIG. 12: We compare the nonspinning BH-absorption Teukolsky-equation flux to the nonspinning Taylor-expanded PN model of Ref. [29] (see Eq. (35)), the $\rho^{\mathrm{H}}_{\ell m}$–factorized model (see Eq. (34)), and the nonspinning limit of the $\tilde{\rho}^{\mathrm{H}}_{\ell m}$–factorized model of this paper. A vertical line marks the ISCO. The curve extend up to the LR.

For the sake of completeness, we list the rest of the $\rho^{\mathrm{H}}_{\ell m}$'s defined in Eq. (34) for $q=0$, which are computed starting from the nonspinning limit of the Taylor-expanded modes:

$$\rho^{\mathrm{H}}_{21}(q=0) = 1 + \frac{19}{12}v^2 + \mathcal{O}(v^4)\,, \qquad (50)$$

$$\rho^{\mathrm{H}}_{33}(q=0) = \rho^{\mathrm{H}}_{31}(q=0) = 1 + \mathcal{O}(v^2)\,, \qquad (51)$$

$$\rho^{\mathrm{H}}_{32}(q=0) = \rho^{\mathrm{H}}_{4m}(q=0) = \mathcal{O}(v)\,. \qquad (52)$$

Lastly, in Fig. 12 we consider the nonspinning limit and compare the BH-absorption total numerical flux to the nonspinning (i) Taylor-expanded PN flux [29], (ii) the $\rho^{\mathrm{H}}_{\ell m}$ factorized flux from Eq. (35) and (iii) the $\tilde{\rho}^{\mathrm{H}}_{\ell m}$ factorized flux proposed in this paper and given in Eq. (41).

V. CONCLUSIONS

Building on Refs. [36–38], we have proposed a new analytical model for the BH-absorption energy flux of a test particle on a circular orbit in the equatorial plane of a Kerr BH. We recast the Taylor-expanded PN flux in a factorized form that allowed us to enforce two key features present in BH perturbation theory: the presence of a zero

at a frequency equal to the frequency of the horizon, and the divergence at the LR. The latter was also adopted for the energy flux at infinity in Refs. [36–38]. These features are not captured by the Taylor-expanded PN flux. We compared our model to the absorption flux computed from the numerical solution of the Teukolsky equation in frequency domain [5–7]. In particular, we computed the gravitational-wave fluxes both at infinity and through the horizon for a Kerr spin $-0.99 \leq q \leq 0.99$, and for the first time down to a radial separation $r = r_{\rm LR} + 0.01M$. This extended previous work [41] to unstable circular orbits below the ISCO.

We investigated the hierarchy of the multipolar flux modes. As the spin grows to large positive values, more and more modes become comparable to the dominant (2,2) mode, even before the ISCO. Among modes with the same value of ℓ, the dominant ones are those with $\ell = |m|$. Close to the LR all modes with $\ell = |m|$ become comparable to the (2,2) mode. We also studied how the mode hierarchy changes at the ISCO frequency when we vary the spin. We found that only the $(2,1)$ and $(3,3)$ modes are always larger than 1% of the $(2,2)$ mode (see Fig. 4); only when $q \gtrsim 0.95$ the (4,4), (5,5), (6,6) and (3,2) modes are above the 1% threshold at the ISCO. One can understand these facts analytically within the WKB approximation, as already pointed out by old studies on geodesic synchrotron radiation [50–53]. One can rewrite the radial Teukolsky equation in a Schrödinger-like form, so that the flux modes turn out to be proportional to a barrier-penetration factor which exponentially suppresses modes with $\ell \neq |m|$.

We compared the numerical fluxes at infinity and through the horizon with the factorized fluxes for several spin values $-0.99 \leq q \leq 0.99$. For the energy flux at infinity, we found that the factorized model developed in Ref. [37] is reliable for retrograde orbits and in the non-spinning case almost up to the LR, but performs rather poorly for large spin prograde orbits close to the LR. For the BH-absorption energy flux we found that the agreement of the factorized flux to the numerical flux is always better than the one of the Taylor-expanded PN flux. The fractional difference between the numerical and factorized flux is less than 1% up to the ISCO for $-1 \leq q \leq 0.5$. For spins $q > 0.7$ the factorized flux starts performing worse, even before the ISCO, but it always performs better than the Taylor-expanded PN flux. We expect that the large modeling error after the ISCO for $q > 0.7$ will not affect much the inspiral, merger and ringdown waveforms produced with the time-domain Teukolsky equation evolved with the factorized flux. In fact, the energy flux does not have much effect beyond the ISCO, since the system's dynamics at that point are well described by a plunging geodesic. In Ref. [45] we show that evolving an EOB dynamics with the factorized model instead of the numerical flux introduces a difference in the time of coalescence smaller than half of a percent across the whole spin range.

Finally, in the Appendices C and D we computed fits to the numerical fluxes at infinity and through the horizon that could be used for highly accurate numerical evolution of EMRIs using PN or EOB equations of motions, and also for modeling the merger waveforms of small mass-ratio binary systems [45].

Future work may address the issue of why the total energy fluxes normalized to the specific energy diverge when computed exactly at the photon orbit. In fact, as we discussed, in this case the WKB treatment suggests a non-convergent sum over the multipolar modes [see Eq. (18)], since the cutoff mode index ℓ_c would go to $+\infty$. This issue is of broader interest, since it is also present in the context of ultrarelativistic BH encounters [54].

In the near future we plan to extend the factorized model of the BH-absorption flux to the case of spinning comparable-mass BHs, so that it can be used in the EOB model when calibrating it to numerical-relativity simulations.

Acknowledgments

We thank Enrico Barausse, Yi Pan and Nico Yunes for useful and informative discussions.

A.B. and A.T. acknowledge partial support from NSF Grants No. PHY-0903631 and No. PHY-1208881. A.B. also acknowledges partial support from the NASA Grant NNX12AN10G and A.T. from the Maryland Center for Fundamental Physics. A.B. and A.T. also thank the hospitality of the Kavli Institute for Theoretical Physics (supported by the NSF Grant No. PHY11-25915) where part of this work was carried out. This work was supported at MIT by NSF Grant PHY-1068720. SAH gratefully acknowledges fellowship support by the John Simon Guggenheim Memorial Foundation, and sabbatical support from the Canadian Institute for Theoretical Astrophysics and the Perimeter Institute for Theoretical Physics. G.K. acknowledges research support from NSF Grant Nos. PHY-1016906, CNS-0959382, PHY-1135664 and PHY-1303724, and from the US Air Force Grant Nos. FA9550-10-1-0354 and 10-RI-CRADA-09.

Appendix A: The Teukolsky-equation source term for light-ring orbits

In this appendix, we describe how the divergence in fluxes at the light ring enters through the Teukolsky equation's source term, as well as a simple modification that allows us to factor it from the flux computation. This divergence-free form proved useful for understanding how fluxes behave in the extreme strong field.

We begin with the stress-energy tensor of a body with rest mass μ moving in the Kerr spacetime:

$$T_{\alpha\beta} = \mu \int u_\alpha u_\beta \, \delta^{(4)}[x^\mu - z^\mu(\tau)] \, d\tau \, . \qquad \text{(A1)}$$

Here, x^μ is a general spacetime coordinate, and $z^\mu(\tau)$ is the worldline followed by the moving body; $u^\alpha = dz^\alpha/d\tau$, where τ is proper time along the worldline. The delta function is normalized so that

$$\int \sqrt{-g}\,\delta^{(4)}\,d^4x = 1\,, \tag{A2}$$

where $g = -\Sigma\sin^2\theta$ is the determinant of the Kerr metric, and $\Sigma = r^2 + q^2M^2\cos^2\theta$.

In a typical particle analysis, we integrate Eq. (A1) immediately to obtain

$$T_{\alpha\beta} = \mu\frac{u_\alpha u_\beta}{\Sigma\sin\theta(dt/d\tau)}\,\delta[r - r(t)]\,\delta[\theta - \theta(t)]\,\delta[\phi - \phi(t)]\,. \tag{A3}$$

This is well-behaved except when $dt/d\tau \to 0$. This occurs at the light ring, and explains why gravitational-wave fluxes diverge as the light ring is approached.

Let us rewrite Eq. (A1) using $d\lambda = d\tau/\mu$, in anticipation of taking the limit $\mu \to 0$. Using the fact that $dz^\alpha/d\lambda = p^\alpha$, the momentum of the body, we find

$$\begin{aligned} T_{\alpha\beta} &= \frac{1}{\mu}\int p_\alpha p_\beta\,\delta^{(4)}[x^\mu - z^\mu(\lambda)](\mu\,d\lambda) \\ &= \int p_\alpha p_\beta\,\delta^{(4)}[x^\mu - z^\mu(\lambda)]\,d\lambda\,. \end{aligned} \tag{A4}$$

This is easily integrated, and we find

$$\begin{aligned} T_{\alpha\beta} &= \frac{p_\alpha p_\beta}{\Sigma\sin\theta\,p^t}\,\delta[r - r(t)]\,\delta[\theta - \theta(t)]\,\delta[\phi - \phi(t)] \\ &= \frac{p_\alpha p_\beta}{\Sigma\,p^t}\,\delta[r - r_{\rm o}]\,\delta[\theta - \pi/2]\,\delta[\phi - \phi(t)]\,. \end{aligned} \tag{A5}$$

On the second line, we specialize to a circular orbit of radius $r = r_{\rm o}$ in the equatorial plane. Equation (A5) is well behaved as $\mu \to 0$.

The momenta which appear in this stress-energy tensor are determined by the geodesic equations for Kerr orbits [48]

$$\begin{aligned} \Sigma\,p^t &= \frac{(r^2+q^2M^2)}{\Delta}\left[E(r^2+q^2M^2) - qML_z\right] \\ &\quad + qM(L_z - qME)\,, \end{aligned} \tag{A6}$$

$$\Sigma\,p^\phi = \frac{qM}{\Delta}\left[E(r^2+q^2M^2) - qML_z\right] + L_z - qME\,, \tag{A7}$$

$$\begin{aligned} (\Sigma\,p^r)^2 &= \left[E(r^2+q^2M^2) - qML_z\right]^2 \\ &\quad - \Delta\left[\mu^2r^2 + (L_z - qME)^2\right]\,. \end{aligned} \tag{A8}$$

We have specialized to $\theta = \pi/2$. This allows us to set the Carter constant $Q = 0$ and to neglect p^θ.

Equations (A6) and (A7) are proportional to the orbiting body's rest mass μ; Eq. (A8) is proportional to μ^2. In most Teukolsky solvers, we factor out the overall factors of μ, and thereby express everything on a per-unit-rest-mass basis. As the light ring is approached, the energy and angular momentum per unit rest mass diverge. In anticipation of this, let us instead divide by the orbital energy E. Defining $\hat{p}^\mu \equiv p^\mu/E$, the stress-energy tensor is written

$$\begin{aligned} T_{\alpha\beta} &= E\,\frac{\hat{p}_\alpha\hat{p}_\beta}{\Sigma\sin\theta\,\hat{p}^t}\,\delta[r - r(t)]\,\delta[\theta - \theta(t)]\,\delta[\phi - \phi(t)] \\ &= E\,\frac{\hat{p}_\alpha\hat{p}_\beta}{\Sigma\,\hat{p}^t}\,\delta[r - r_0]\,\delta[\theta - \pi/2]\,\delta[\phi - \phi(t)]\,, \end{aligned} \tag{A9}$$

where again the second line is specialized to an equatorial, circular orbit. The momenta appearing here are given by

$$\begin{aligned} \Sigma\,\hat{p}^t &= \frac{(r^2+q^2M^2)}{\Delta}\left[(r^2+q^2M^2) - qMb\right] \\ &\quad + qM(b - qM)\,, \end{aligned} \tag{A10}$$

$$\Sigma\,\hat{p}^\phi = \frac{qM}{\Delta}\left[(r^2+q^2M^2) - qMb\right] + b - qM\,, \tag{A11}$$

$$\begin{aligned} (\Sigma\,\hat{p}^r)^2 &= \left[(r^2+q^2M^2) - qMb\right]^2 \\ &\quad - \Delta\left[\frac{r^2}{\hat{E}^2} + (b - qM)^2\right]\,. \end{aligned} \tag{A12}$$

We have introduced the orbit's energy per unit rest mass $\hat{E} \equiv E/\mu$ and the orbit's "impact parameter" $b \equiv L_z/E$ [see Eqs. (29)–(30)]. These expressions work well all the way to the light ring, Eq. (15).

To implement this form of the source, we follow the recipe outlined in Sec. IV of Ref. [5] [see especially Eqs. (4.32) – (4.34)], but using Eq. (A9) instead of Eq. (A3). The code then computes the amplitudes $Z^\star_{\ell m}$ per unit orbital energy rather than per unit rest mass, and hence computes all fluxes per unit orbital energy squared. This factors out the divergence associated with the behavior of the energy per unit mass at the light ring.

When this is done, each modal contribution $F^\star_{\ell m}$ is perfectly well behaved at the light ring. The sum of all modes can grow quite large, but only because there are many modes that contribute, not because of the pole at the light ring.

Appendix B: Expressions for $\tilde{f}^{\rm H}_{\ell m}$

In this appendix we write the explicit expressions of the $\tilde{f}^{\rm H}_{\ell m}$ polynomials. We find

$$\tilde{f}^{\rm H}_{22} = 1 + 2v^2 - \left\{4B_2 + \frac{2q}{\kappa\left(1+3q^2\right)}\left[5+4\kappa - q^2\left(2+3q^2\right)\right]\right\}v^3 + \left(\frac{377}{42} - \frac{8}{42}q^2\right)v^4$$
$$- \left\{8B_2 + \frac{q}{1+3q^2}\left[\frac{119}{9} - \frac{25}{3}q^2 + 4\kappa\left(5+3q^2\right)\right]\right\}v^5 + \left\{\frac{547\,402}{11\,025} - \frac{4}{3}\pi^2 - \frac{7\,942}{567}q^2 + 2q^4 + 8B_2^2\right.$$
$$+ 8C_2\left(1+\frac{2}{\kappa}\right) - \frac{856}{105}\left(A_2 + \gamma_E + \log 2 + \log\kappa + 2\log v\right) - \frac{1}{1+3q^2}\left[\frac{152}{9} - 32qB_2 - 8q\kappa B_2\left(5+3q^2\right)\right]$$
$$\left. + \frac{1}{\left(1+3q^2\right)^2}\left[\frac{224}{9} + 4\kappa\left(5+4q^2+9q^4-18q^6\right)\right]\right\}v^6 - \left[-\frac{1\,641}{189}q + \frac{73}{189}q^3 + \frac{4\,556q}{63\left(1+3q^2\right)}\right.$$
$$\left. + \frac{1}{21}\left(377-8q^2\right)\left(2B_2 + q\kappa\frac{5+3q^2}{1+3q^2}\right)\right]v^7 + \left\{\frac{4\,579\,699}{33\,075} - \frac{8}{3}\pi^2 - \frac{14\,617}{567}q^2 + \frac{529}{126}q^4 - \frac{5\,296}{105}\gamma_E - \frac{1\,712}{105}A_2\right.$$
$$+ 16B_2^2 + 16C_2\left(1+\frac{2}{\kappa}\right) - \frac{100}{9}qB_2 + \frac{1}{1+3q^2}\left[-\frac{712}{27} + 64qB_2 + 16\kappa qB_2\left(5+3q^2\right)\right] + \frac{1}{\left(1+3q^2\right)^2}$$
$$\left.\times\left[\frac{448}{9} + \kappa\left(40 + \frac{38}{9}q^2 - 28q^4 - 194q^6\right)\right] - \frac{592}{7}\log 2 - \frac{1\,712}{105}\log\kappa - \frac{2\,336}{35}\log v\right\}v^8 + \mathcal{O}(v^9)\,, \tag{B1a}$$

$$\tilde{f}^{\rm H}_{21} = 1 - \frac{2}{3}qv + \frac{7}{6}v^2 + \left\{-2B_1 + \frac{2q}{4-3q^2}\left[\frac{5}{3} - 2q^2 - \kappa\left(5-3q^2\right)\right]\right\}v^3 + \left\{\frac{841}{504} + \frac{4}{3}qB_1\right.$$
$$\left. - \frac{1\,165}{378}q^2 + \frac{4}{3\left(4-3q^2\right)}\left[\frac{4}{3} + q^2\kappa\left(5-3q^2\right)\right]\right\}v^4 + \left\{\frac{785}{252}q + \frac{13}{14}q^3 - \frac{7}{3}\left[B_1 + \frac{q}{4-3q^2}\left[1+\kappa\left(5-3q^2\right)\right]\right]\right\}v^5$$
$$+ \left\{\frac{303\,727}{19\,600} - \frac{12\,055}{2\,268}q^2 + 2q^4 - \frac{\pi^2}{3} - \frac{214}{105}\left(A_1 + \gamma_E + \log 2 + \log\kappa + 2\log v\right) + 2B_1^2\right.$$
$$+ 2C_1\left(1+\frac{2}{\kappa}\right) - \frac{1}{4-3q^2}\left[\frac{40}{9} - 4qB_1\left(-\frac{5}{3} + 2q^2 + \kappa\left(5-3q^2\right)\right)\right] + \frac{16}{3\left(4-3q^2\right)^2}\left[\kappa\left(15 - 52q^2\right.\right.$$
$$\left.\left.\left. + 54q^4 - 18q^6\right) - \frac{1}{3}\right]\right\}v^6 + \mathcal{O}(v^7)\,, \tag{B1b}$$

$$\tilde{f}^{\rm H}_{33} = 1 + \frac{7}{2}v^2 - \left\{6B_3 + \frac{q}{\left(1+8q^2\right)\left(4+5q^2\right)}\left[\frac{262}{3} + \frac{628}{3}q^2 - \frac{80}{3}q^4 + 18\kappa\left(5+13q^2\right)\right]\right\}v^3$$
$$+ \left(\frac{1\,549}{120} - \frac{5}{6}q^2\right)v^4 + \mathcal{O}(v^5)\,, \tag{B2a}$$

$$\tilde{f}^{\rm H}_{32} = 1 - \frac{3}{4}qv + \frac{5}{2}v^2 + \mathcal{O}(v^3)\,, \tag{B2b}$$

$$\tilde{f}^{\rm H}_{31} = 1 + \frac{29}{6}v^2 - 2\left\{B_1 + \frac{q}{4-3q^2}\left[\kappa\left(5-3q^2\right) + \frac{1}{9-8q^2}\left(65 - \frac{866}{9}q^2 + \frac{104}{3}q^4\right)\right]\right\}v^3$$
$$+ \left(\frac{1\,195}{72} + \frac{1}{2}q^2\right)v^4 + \mathcal{O}(v^5)\,, \tag{B2c}$$

$$\tilde{f}^{\rm H}_{44} = 1 + \mathcal{O}(v)\,, \tag{B3a}$$
$$\tilde{f}^{\rm H}_{43} = \mathcal{O}(v)\,, \tag{B3b}$$
$$\tilde{f}^{\rm H}_{42} = 1 + \mathcal{O}(v)\,, \tag{B3c}$$
$$\tilde{f}^{\rm H}_{41} = \mathcal{O}(v)\,. \tag{B3d}$$

We have compared the factorized fluxes built using either the $\tilde{\rho}^{\rm H}_{\ell m}$'s or $\tilde{f}^{\rm H}_{\ell m}$'s against the Teukolsky-equation flux and have found that the latter have fractional differences one order of magnitude smaller than the former for prograde orbital geometries. For retrograde orbits, instead, the two factorizations have more similar modeling errors.

For this reason we have employed the $\tilde{\rho}^{\rm H}_{\ell m}$–factorization in the paper.

Appendix C: Fits of the gravitational flux at infinity

In this appendix we fit the gravitational flux at infinity computed through the Teukolsky equation to further improve the amplitude of the factorized modes, given in Eq. (31), and the total factorized flux. The Teukolsky-equation data available to us span frequencies from $v = 0.01$ up to $r = r_{\rm LR} + 0.01M$, and have spins in the range $q \in \{-0.99, -0.95, -0.9, -0.8, -0.7, -0.6, -0.5, -0.4, -0.3, -0.2, -0.1, 0, 0.1, 0.2, 0.3, 0.4, 0.5, 0.6, 0.7, 0.8, 0.9, 0.95, 0.99\}$.

Improving the mode's amplitude $|h_{lm}|$'s (which is equivalent to improving the mode's flux F^{∞}_{lm}) is conducive to the EOB modeling of the merger signal in the small mass-ratio limit for large spins, which we have pursued in Ref. [45]. [Note that the modes in this appendix are spherical-harmonic modes, labeled (l, m).] Earlier efforts in this direction (e.g., see Refs. [41, 43]) were plagued by significant modeling errors in the $|h_{lm}|$'s for spins $q \gtrsim 0.7$. For such systems, the discrepancies between time-domain Teukolsky-equation waveforms and EOB waveforms showed up early on during the adiabatic inspiral, where non-quasi-circular effects are still negligible. This had also the effect of introducing a large error on the total F^{∞}, which depends on the $|h_{lm}|$'s through Eq. (26).

We perform the fit by adding to the ρ_{lm}'s of Ref. [37] an additional term $\rho^{\rm amp\,fit}_{lm}$, which is determined by the fit. We fit the minimal number of unknown higher PN orders beyond the current analytical knowledge of the ρ_{lm}'s, such that the residuals on the individual F^{∞}_{lm} (or, equivalently, on $|h_{lm}|$) are within 5% up to the ISCO. It is worth reminding that Ref. [37] based their factorized model on unpublished Taylor-expanded modes computed in BH perturbation theory by Tagoshi and Fujita. In previous years, Ref. [60] had derived the Taylor-expanded modes needed to compute the 5.5PN energy flux at infinity for the Schwarzschild case, while Ref. [61] had derived the Taylor-expanded modes needed to compute the 4PN energy flux at infinity for a particle in the equatorial plane of a Kerr BH. However, in both instances, the explicit formulae had not been published. Reference [62] independently derived the nonspinning Taylor-expanded multipolar waveforms up to 5.5PN order, and computed a $\rho_{lm}-$factorization which includes some higher PN nonspinning terms as compared to Ref. [37]. Reference [37] itself pointed out (before Eq. (A1)) that their nonspinning ρ_{lm}'s agreed with those of Ref. [62] only up to $\mathcal{O}(v^{11-2(l-2)})$. References [63] and [64] pushed the computation of the energy flux at infinity for Schwarzschild up to 14PN and 22PN order respectively, but provided only the 6PN term entering the ρ_{22}. Again, for the rest of this appendix we will build upon the analytical results of Ref. [37].

Table I of Ref. [37] lists the PN knowledge of the different modes h_{lm}'s at the time of publication. In particular, given (l, m), from the second line of that table one can read the available PN order beyond the leading term $h^{(N,\epsilon)}_{lm}$ for the Taylor-expanded expression of the mode, with a distinction between nonspinning and spinning terms. It turns out that when $l \leq 5$ the nonspinning sector is known to a higher or equal PN order than the spinning sector; on the other hand, when $l > 5$ the knowledge of the spinning terms is better than the nonspinning ones.

As already pointed out in Refs. [37, 43, 56, 65], the larger the value of q, the more multipolar modes become comparable with the dominant (2,2) mode: see Fig. 3 of Ref. [43], which shows the mode hierarchy for $q = 0, 0.9$ based on their amplitude $|h_{lm}|$. An analytical explanation for the hierarchy of the modes can also be found using the WKB approximation [50–53]. The multipolar modes we fit are: (2,2), (2,1), (3,3), (3,2), (3,1), (4,4), (4,3), (4,2), (5,5), (5,4), (6,6), (7,7) and (8,8).

Note that we perform the fits in the domain of the orbital velocity $v \equiv (M\Omega)^{1/3}$, over the restricted range $0.01 \leq v \leq v_{\rm ISCO}$ (where $v_{\rm ISCO} \equiv (M\Omega_{\rm ISCO})^{1/3} = [(r_{\rm ISCO}/M)^{3/2}+q]^{-1/3}$). The reason for doing so (instead of going up to the final available frequency) is threefold: i) from the point of view of the waveform, our primary goal is to improve the adiabatic analytical model and modeling errors in the plunge amplitude can easily be fixed by introducing non-quasi-circular corrections [45]; ii) from the point of view of the energy flux at infinity, after the ISCO the orbital motion of the binary becomes basically geodetic![9]; iii) we find it difficult to fit well the post-ISCO data, all the way to the LR without spoiling the low-frequency portion of the fit. As to the spin range covered, we cannot include $q = 0.99$ without affecting in a negative way smaller spins. While computing the fits, we give equal weight to all available spins, and fit them all together. This is achieved by rescaling each range $0.01 \leq v \leq v_{\rm ISCO}$ such that they all have the same measure, and by stitching together all different ranges. We also tried fits in the domain of the orbital frequency $M\Omega$, which amounts to giving more importance to higher frequencies, but this created large relative errors at lower frequencies, where the binary spends the majority of the time, therefore increasing the phase error due to the flux modeling.

Table III lists the fitted functions $\rho^{\rm amp\,fit}_{lm}$. In those expressions we use $\text{eulerlog}_m x \equiv \log\gamma_E + \log 2m + \log\sqrt{x}$ ($\gamma_E \approx 0.577215\ldots$ being Euler's constant).

For multipolar modes with $l \leq 4$ the fitting functions contain only spinning terms. But starting from $l = 5$

[9] The plunge lasts for a time $\mathcal{O}(M)$, in contrast to the inspiral, which lasts for a much longer time $\mathcal{O}(M^2/\mu)$ [66, 67]. Therefore the motion of the plunging particle is well approximated by a geodesic in Kerr spacetime.

(l,m)	$\rho_{lm}^{\rm amp\,fit}$	rel. err.
(2, 2)	$(-20.28 + 12.03\,\mathrm{eulerlog}_2 v^2)\,qv^9$	$\lesssim 0.3\%$
(2, 1)	$(-0.5144 + 3.175\,\mathrm{eulerlog}_1 v^2)\,q^2v^8$	$\lesssim 0.4\%$
(3, 3)	$3.894\,q^2v^8 + (-42.08 + 12.76\,\mathrm{eulerlog}_3 v^2)\,qv^9$	$\lesssim 0.2\%$
(3, 2)	$-0.6932\,qv^7 - 1.558\,q^2v^8$	$\lesssim 1\%$
(3, 1)	$-1.012\,q^2v^8 + (0.8846 - 1.279\,\mathrm{eulerlog}_1 v^2)\,qv^9$	$\lesssim 0.08\%$
(4, 4)	$0.9625\,qv^7 + (-2.069 - 0.7846\,\mathrm{eulerlog}_4 v^2)\,v^8 - 0.2633\,q^2v^8$	$\lesssim 0.2\%$
(4, 3)	$1.424\,q^2v^6 - 2.475\,qv^7$	$\lesssim 0.8\%$
(5, 5)	$(19.51 - 5.623\,\mathrm{eulerlog}_5 v^2)\,v^6 + 0.3443\,q^2v^6$	$\lesssim 1\%$
(6, 6)	$-0.9925\,qv^5 - 0.03416\,q^2v^6 + (19.75 - 5.328\,\mathrm{eulerlog}_6 v^2)\,v^6$	$\lesssim 0.8\%$
(7, 7)	$-1.732\,v^4 + 0.4912\,q^2v^4 - 1.117\,qv^5 + 0.1468\,q^2v^6 + (25.63s - 6.979\,\mathrm{eulerlog}_7 v^2)\,v^6$	$\lesssim 0.2\%$
(8, 8)	$-0.9946\,qv^3 - 0.2949\,v^4 + 0.003748\,q^2v^4 + 2.428\,qv^5$	$\lesssim 1.2\%$

TABLE III: Functions $\rho_{lm}^{\rm amp\,fit}$ fitted to individual multipolar modes of the numerical flux at infinity. The coefficients are given with 4 significant figures. In the last column we show the upper bound on the residual relative error of these fits over the spin and frequency ranges used for the fits, i.e. all spins except $q = 0.99$, and up to the ISCO.

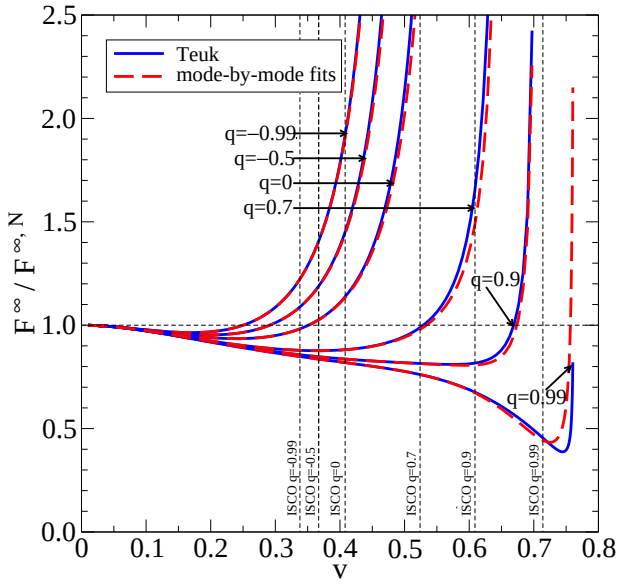

FIG. 13: We plot the total Teukolsky-equation flux at infinity (in solid blue) and the ρ_{lm}–factorized model of Ref. [37], improved with the amplitude fits $\rho_{lm}^{\rm amp\,fit}$ (in dashed red). The curves extend up to $r = r_{\rm LR} + 0.01M$. The fluxes are normalized by the leading quadrupole luminosity at infinity.

both nonspinning and spinning terms are fitted. For instance, for the (5,5) mode, both the nonspinning and spinning sector are known through 2.5PN beyond the leading order, therefore we fit both sectors at 3PN order.

The choice of including logarithmic terms or not is based on the patterns displayed by the currently available expressions for the ρ_{lm}'s: nonspinning (spinning) logarithmic terms show up at 3PN order beyond the leading nonspinning (spinning) term. We also choose the spin dependence for the spinning terms to be either linear of quadratic in q, again based on the patterns present in the ρ_{lm}'s: spinning terms proportional to odd (even) powers of v are odd (even) in the spin q.

Finally, the (7,7) and (8,8) modes turn out to be quite difficult to fit, due to the limited Taylor-expanded knowledge from BH perturbation theory, and they require as many as 3 PN orders to be fitted within a few percent accuracy, which means a total of 6 fitting parameters for (7,7) and 4 fitting parameters for (8,8). In contrast, all other modes with $l \leq 6$ can be accurately fitted using only half or one PN order. We end up fitting a total of 35 coefficients.

The quality of the fits is generally very good on a mode-by-mode basis, with residuals always smaller than $\sim 1.2\%$ for all the values of q (except 0.99), for frequencies up to the ISCO and for all the fitted multipolar modes. In the third column of Table III we list the upper bound for the relative error on the fits of the multipolar modes.

We now turn to the total energy flux at infinity. In Fig. 13 we show comparisons of $F^{\infty}_{\rm Teuk}$ against the model with the mode-by-mode fits discussed above. When the spins are negative or small, the factorized model of Ref. [37] actually performs fairly well without any additional fit: for those cases, in fact, the modeling error is less that 1% at the ISCO, as demonstrated by Fig. 5. In general, the energy flux diverges at the LR since the energy-momentum tensor of the particle sourcing the GW perturbations diverges there as well. This feature is incorporated in the model through the effective source factor $\hat{S}^{(\epsilon)}_{\rm eff}$, which behaves like $(r - r_{\rm LR})^{-1}$ for $r \sim r_{\rm LR}$ [35–37]. But, when the spin is large and positive, the divergence of the numerical flux is localized in a narrow neighborhood of the LR, while the model without fits starts growing to large values even before the ISCO. For instance, when $q \geq 0.9$, the factorized model differs from the numerical data by more than 100% even before the ISCO, so that an EOB evolution based on such

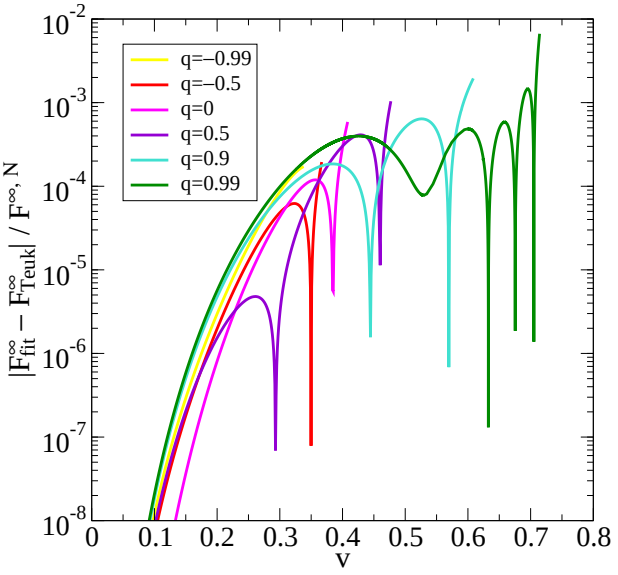

FIG. 14: We show the absolute residual error (normalized by the leading order luminosity at infinity) on the factorized flux at infinity improved with $\rho^{\rm amp\,fit}_{lm} + \rho^{\rm tot\,fit}_{lm}$. All curves extend up to the respective ISCOs.

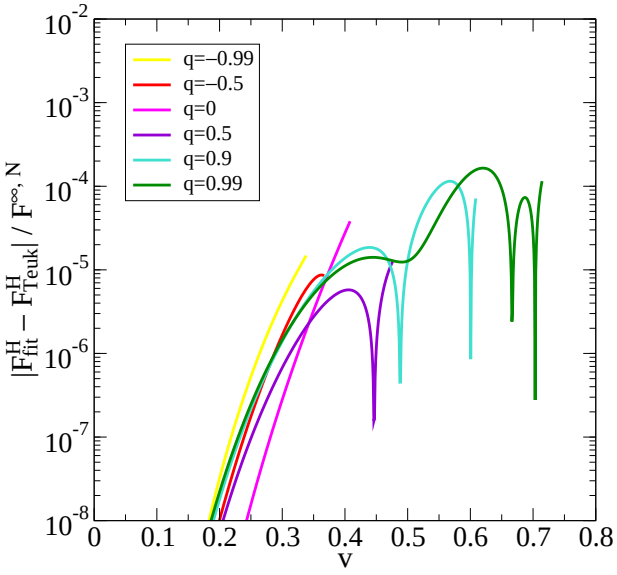

FIG. 15: We show the absolute residual error on the fitted absorption flux, normalized by the leading order luminosity at infinity. All curves extend up to the respective ISCOs.

flux would be unreliable already in the late inspiral, as already pointed out earlier. When the fits are included, the model agrees with the numerical data to within 0.1% before the ISCO for all the spins up to $q = 0.99$, as shown in Fig. 13.

As a final refinement, on top of the mode-by-mode fits just discussed, we add 8 additional fitting parameters (4 in the (2,2) mode, 4 in the (3,3) mode), and determine them through a global fit on F^{∞} itself, similarly to what Refs. [41, 68] did. Again we restrict to $0.01 \leq v \leq v_{\rm ISCO}$, but now we include also $q = 0.99$. We can achieve a reduction of the error by about an order of magnitude at the ISCO for all the available spins, as shown in Fig. 14. These additional terms to be added to $\rho_{lm} + \rho^{\rm amp\,fit}_{lm}$, which we will call $\rho^{\rm tot\,fit}_{lm}$, read

$$\begin{aligned}
\rho^{\rm tot\,fit}_{22} &= (-9.890 + 9.039\,{\rm eulerlog}_2 v^2)\,q^2 v^{10} \\
&+ (-18.84 + 2.486\,{\rm eulerlog}_2 v^2)\,q v^{11}\,, \quad \text{(C1)} \\
\rho^{\rm tot\,fit}_{33} &= [73.73 - 36.97\,{\rm eulerlog}_3 v^2 \\
&+ q^2\,(3.955 - 0.7106\,{\rm eulerlog}_3 v^2)]\,v^{10}\,. \quad \text{(C2)}
\end{aligned}$$

Appendix D: Fits of the black-hole absorption gravitational flux

In this appendix we provide numerical fits to the Teukolsky-equation black-hole absorption fluxes. Our starting point is the $\tilde{\rho}^{\rm H}_{\ell m}$–factorized model developed in this paper. We add to the $\tilde{\rho}^{\rm H}_{\ell m}$'s in Eqs. (42)–(44) higher-order PN terms $\tilde{\rho}^{\rm H,fit}_{\ell m}$. In particular, we modify only the dominant and leading subdominant modes (2,2), (2,1) and (3,3). We choose the functional form of the $\tilde{\rho}^{\rm H,fit}_{\ell m}$'s based on the lower PN orders, trying to include similar dependences on v and q. We have data for the Teukolsky-equation $F^{\rm H}$ for as many as 22 spins: $q \in \{-0.99, -0.9, -0.8, -0.7, -0.6, -0.5, -0.4, -0.3, -0.2, -0.1, 0, 0.1, 0.2, 0.3, 0.4, 0.5, 0.6, 0.7, 0.8, 0.9, 0.95, 0.99\}$. The fits are done globally on all spins in v–space. The sampled frequency ranges extend from $v = 0.01$ up to $r = r_{\rm LR} + 0.01M$, but we use data only up $r = (r_{\rm ISCO} + r_{\rm LR} + 0.01M)/2$, since attempts to include the whole available velocity ranges spoil the lower frequency portion of the fits; nonetheless our fits prove very accurate up to the ISCO. In order to have residual relative errors within a few percent for all the available spins up to the ISCO, we have to use 11 fitting coefficients. We find

$$\begin{aligned}
\tilde{\rho}^{\rm H,fit}_{22} &= -(1570 + 118.5\,q + 589.7\,\log v)\,v^9 \\
&+ (1323 + 336.3\,q - 1291\,\log v)\,v^{10}\,, \quad \text{(D1)} \\
\tilde{\rho}^{\rm H,fit}_{21} &= (50.25 - 54.95\,q - 40.39\,\log v)\,v^7\,, \quad \text{(D2)} \\
\tilde{\rho}^{\rm H,fit}_{33} &= (15.65 - 13.41\,q)\,v^5\,. \quad \text{(D3)}
\end{aligned}$$

Figure 15 shows what are the residuals on the fitted ingoing fluxes, normalized by the leading order luminosity at infinity. We plot this quantity, rather than the relative residual errors, because in any realistic setting these fits are going to be added into a radiation reaction term where the flux at infinity is also present. In fact, as discussed before (see Fig. 1), $|F^{\rm H}|$ is always much smaller than $|F^{\infty}|$ before the ISCO, and one is typically interested in an accurate total flux ($F^{\infty} + F^{\rm H}$), hence our choice of the normalization. It is therefore possible to estimate the modeling error on the total flux by directly

adding Fig. 14 and Fig. 15.

[1] P. Amaro-Seoane, J. R. Gair, M. Freitag, M. Coleman Miller, I. Mandel, et al., Class.Quant.Grav. **24**, R113 (2007), astro-ph/0703495.
[2] L. Barack, Class.Quant.Grav. **26**, 213001 (2009), 0908.1664.
[3] E. Poisson, A. Pound, and I. Vega, Living Rev.Rel. **14**, 7 (2011), 1102.0529.
[4] S. A. Teukolsky, Astrophys.J. **185**, 635 (1973).
[5] S. A. Hughes, Phys.Rev. **D61**, 084004 (2000), gr-qc/9910091.
[6] S. A. Hughes, Phys.Rev. **D64**, 064004 (2001), gr-qc/0104041.
[7] S. Drasco and S. A. Hughes, Phys.Rev. **D73**, 024027 (2006), gr-qc/0509101.
[8] C. Cutler, E. Poisson, G. Sussman, and L. Finn, Phys.Rev. **D47**, 1511 (1993).
[9] C. Cutler, D. Kennefick, and E. Poisson, Phys.Rev. **D50**, 3816 (1994).
[10] K. Glampedakis and D. Kennefick, Phys.Rev. **D66**, 044002 (2002), gr-qc/0203086.
[11] M. Sasaki and H. Tagoshi, Living Rev.Rel. **6**, 6 (2003), gr-qc/0306120.
[12] T. Futamase and Y. Itoh, Living Rev.Rel. **10**, 2 (2007).
[13] L. Blanchet, Living Rev.Rel. **9**, 4 (2006).
[14] I. Mandel and J. R. Gair, Class.Quant.Grav. **26**, 094036 (2009), 0811.0138.
[15] C. W. Misner, Phys.Rev.Lett. **28**, 994 (1972).
[16] R. Penrose, Riv.Nuovo Cim. **1**, 252 (1969).
[17] W. H. Press and S. A. Teukolsky, Nature **238**, 211 (1972).
[18] S. Hod, Phys. Rev. **D86**, 104026 (2012).
[19] S. Teukolsky and W. Press, Astrophys.J. **193**, 443 (1974).
[20] S. L. Detweiler, Astrophys.J. **225**, 687 (1978).
[21] S. J. Kapadia, D. Kennefick, and K. Glampedakis (2013), 1302.1016.
[22] V. Cardoso, S. Chakrabarti, P. Pani, E. Berti, and L. Gualtieri, Phys.Rev.Lett. **107**, 241101 (2011), 1109.6021.
[23] V. Cardoso and P. Pani, Class.Quant.Grav. **30**, 045011 (2013), 1205.3184.
[24] J. B. Hartle, Phys.Rev. **D8**, 1010 (1973).
[25] J. B. Hartle, Phys.Rev. **D9**, 2749 (1974).
[26] K. S. Thorne, R. H. Price, and D. A. MacDonald, *Black Holes: The Membrane Paradigm* (Yale University Press, New Haven and London, 1986), 1st ed.
[27] E. Poisson and M. Sasaki, Phys.Rev. **D51**, 5753 (1995), gr-qc/9412027.
[28] H. Tagoshi, S. Mano, and E. Takasugi, Prog.Theor.Phys. **98**, 829 (1997), gr-qc/9711072.
[29] Y. Mino, M. Sasaki, M. Shibata, H. Tagoshi, and T. Tanaka, Prog.Theor.Phys.Suppl. **128**, 1 (1997), gr-qc/9712057.
[30] K. Alvi, Phys.Rev. **D64**, 104020 (2001), gr-qc/0107080.
[31] E. Poisson, Phys.Rev. **D70**, 084044 (2004), gr-qc/0407050.
[32] S. Taylor and E. Poisson, Phys.Rev. **D78**, 084016 (2008), 0806.3052.
[33] K. Chatziioannou, E. Poisson, and N. Yunes (2012), 1211.1686.
[34] U. Sperhake, E. Berti, V. Cardoso, and F. Pretorius (2012), 1211.6114.
[35] T. Damour and A. Nagar, Phys.Rev. **D76**, 064028 (2007), 0705.2519.
[36] T. Damour, B. R. Iyer, and A. Nagar, Phys.Rev. **D79**, 064004 (2009), 0811.2069.
[37] Y. Pan, A. Buonanno, R. Fujita, E. Racine, and H. Tagoshi, Phys.Rev. **D83**, 064003 (2011), 1006.0431.
[38] A. Nagar and S. Akcay, Phys.Rev. **D85**, 044025 (2012), 1112.2840.
[39] S. Bernuzzi and A. Nagar, Phys.Rev. **D81**, 084056 (2010), 1003.0597.
[40] S. Bernuzzi, A. Nagar, and A. Zenginoglu, Phys.Rev. **D83**, 064010 (2011), 1012.2456.
[41] N. Yunes, A. Buonanno, S. A. Hughes, Y. Pan, E. Barausse, M. C. Miller, and W. Throwe, Phys.Rev. **D83**, 044044 (2011), 1009.6013.
[42] S. Bernuzzi, A. Nagar, and A. Zenginoglu, Phys.Rev. **D84**, 084026 (2011), 1107.5402.
[43] E. Barausse, A. Buonanno, S. A. Hughes, G. Khanna, S. O'Sullivan, and Y. Pan, Phys.Rev. **D85**, 024046 (2012), 1110.3081.
[44] S. Bernuzzi, A. Nagar, and A. Zenginoglu, Phys.Rev. **D86**, 104038 (2012), 1207.0769.
[45] A. Taracchini, A. Buonanno, S. A. Hughes, and G. Khanna (2013), in preparation.
[46] R. Fujita and H. Tagoshi, Prog.Theor.Phys. **112**, 415 (2004), gr-qc/0410018.
[47] R. Fujita and H. Tagoshi, Prog.Theor.Phys. **113**, 1165 (2005), 0904.3818.
[48] J. M. Bardeen, W. H. Press, and S. A. Teukolsky, Astrophys.J. **178**, 347 (1972).
[49] W. Throwe and S. A. Hughes (2013), in preparation.
[50] M. Davis, R. Ruffini, J. Tiomno, and F. Zerilli, Phys.Rev.Lett. **28**, 1352 (1972).
[51] R. Breuer, R. Ruffini, J. Tiomno, and C. Vishveshwara, Phys.Rev. **D7**, 1002 (1973).
[52] P. Chrzanowski and C. W. Misner, Phys.Rev. **D10**, 1701 (1974).
[53] R. A. Breuer, ed., *Gravitational perturbation theory and synchrotron radiation*, vol. 44 of *Lecture Notes in Physics, Berlin Springer Verlag* (1975).
[54] E. Berti, V. Cardoso, T. Hinderer, M. Lemos, F. Pretorius, et al., Phys.Rev. **D81**, 104048 (2010), 1003.0812.
[55] S. A. Hughes, Class.Quant.Grav. **18**, 4067 (2001), gr-qc/0008058.
[56] L. S. Finn and K. S. Thorne, Phys.Rev. **D62**, 124021 (2000), gr-qc/0007074.
[57] R. Breuer, P. Chrzanowksi, H. Hughes, and C. W. Misner, Phys.Rev. **D8**, 4309 (1973).
[58] Z. Zhang, N. Yunes, and E. Berti, Phys.Rev. **D84**, 024029 (2011), 1103.6041.
[59] S. Teukolsky, Phys.Rev.Lett. **29**, 1114 (1972).
[60] T. Tanaka, H. Tagoshi, and M. Sasaki, Prog.Theor.Phys. **96**, 1087 (1996), gr-qc/9701050.
[61] H. Tagoshi, M. Shibata, T. Tanaka, and M. Sasaki, Phys.Rev. **D54**, 1439 (1996), gr-qc/9603028.
[62] R. Fujita and B. R. Iyer, Phys.Rev. **D82**, 044051 (2010),

1005.2266.
[63] R. Fujita (2011), 1104.5615.
[64] R. Fujita, Prog.Theor.Phys. **128**, 971 (2012), 1211.5535.
[65] E. Barausse, V. Cardoso, and G. Khanna, Phys.Rev. **D84**, 104006 (2011), 1106.1692.
[66] A. Buonanno and T. Damour, Phys.Rev. **D62**, 064015 (2000), gr-qc/0001013.
[67] Y. Mino and J. Brink, Phys.Rev. **D78**, 124015 (2008), 0809.2814.
[68] J. R. Gair and K. Glampedakis, Phys.Rev. **D73**, 064037 (2006), gr-qc/0510129.